Materials Today Bio 21 (2023) 100692

Contents lists available at ScienceDirect

Materials Today Bio

journal homepage: www.journals.elsevier.com/materials-today-bio

Preparation of co-electrospinning membrane loaded with simvastatin and substance P to accelerate bone regeneration by promoting cell homing, angiogenesis and osteogenesis

Mohammed A. Al-Baadani [a], Lihua Xu [c], Kexin Cai [a], Kendrick Hii Ru Yie [a], Yiding Shen [a], Abdullrahman M. Al-Bishari [a], Bilal A. Al-Shaaobi [a], Pingping Ma [a,***], Xinkun Shen [b,**], Jinsong Liu [a,*]

[a] School and Hospital of Stomatology, Wenzhou Medical University, Wenzhou, 325027, People's Republic of China
[b] Science and Education Division, The Third Affiliated Hospital of Wenzhou Medical University (Ruian People's Hospital), Wenzhou, 325016, People's Republic of China
[c] Department of Stomatology, The First Affiliated Hospital of Wenzhou Medical University, Wenzhou, 325016, People's Republic of China

ARTICLE INFO

Keywords:
Co-electrospinning
MSCs recruitment
Angiogenesis
Osteogenesis

ABSTRACT

Bone regeneration is a complex process that requires the coordination of various biological events. Developing a tissue regeneration membrane that can regulate this cascade of events is challenging. In this study, we aimed to fabricate a membrane that can enrich the damaged area with mesenchymal stem cells, improve angiogenesis, and continuously induce osteogenesis. Our approach involved creating a hierarchical polycaprolactone/gelatin (PCL/GEL) co-electrospinning membrane that incorporated substance P (SP)-loaded GEL fibers and simvastatin (SIM)-loaded PCL fibers. The membrane could initiate a burst release of SP and a slow/sustained release of SIM for over a month. *In vitro* experiments, including those related to angiogenesis and osteogenesis (e.g., migration, endothelial network formation, alkaline phosphatase activity, mineralization, and gene expression), clearly demonstrated the membrane's superior ability to improve cell homing, revascularization, and osteogenic differentiation. Furthermore, a series of *in vivo* studies, including immunofluorescence of $CD29^{+}/CD90^{+}$ double-positive cells and immunohistochemical staining for CD34 and vWF, confirmed the co-electrospinning membrane's ability to enhance MSC migration and revascularization response after five days of implantation. After one month, the Micro-CT and histological (Masson and H&E) results showed accelerated bone regeneration. Our findings suggest that a co-electrospinning membrane with time-tunable drug delivery could advance the development of tissue engineering therapeutic strategies and potentially improve patient outcomes.

1. Introduction

In the last decade, researchers have shown increased interest in bone tissue engineering and have widely investigated the different approaches to making an osteoinductive scaffolds [1]. Guided bone regeneration (GBR) is a common technique in treating critical bone defects, particularly in the cranial region [2]. One of the basic principles of these scaffolds is to prevent the fast-growing soft tissue from penetrating the sealed-off defect area, in which they function as a mechanical barrier. At the same time, this ensures the time to enable the osteoblast cells to proliferate and differentiate in the damaged area [3]. Conventional electrospinning is a simple technique for fabricating GBR membranes (GBRm) using various polymers (natural or synthetic). The acquired membranes are flexible and biodegradable, so they can be left in place without requiring a second surgery to be removed [4]. However, the lack of osteoinductive ability of these membranes and the insufficient regenerative capacity of the bone itself correspondingly determine the unsatisfactory amount of new bone formed after injury [5]. Therefore, the current research and development initiatives concentrate on creating a bioactive GBRm that serves as an impediment scaffold while also delivering bioactive components to accelerate bone reformation at the defect site [6].

* Corresponding author. 268# Xueyuan West Road, Lucheng District, Wenzhou City, Zhejiang Province, People's Republic of China.
** Corresponding author. 108# Wansong Road, Ruian City, Zhejiang Province, People's Republic of China.
*** Corresponding author. Xueyuan West Road, Lucheng District, Wenzhou City, Zhejiang Province, People's Republic of China.
E-mail addresses: ppma2012@sina.com (P. Ma), shenxinkun123@wmu.edu.cn (X. Shen), jinsong0719@wmu.edu.cn (J. Liu).

https://doi.org/10.1016/j.mtbio.2023.100692
Received 11 February 2023; Received in revised form 23 May 2023; Accepted 5 June 2023
Available online 25 June 2023

Researchers have invented a unique approach using fiber membranes as drug carriers. This approach provided a localized drug delivery into the target site and significantly improved the function of the osteogenic-related cells in the protected space below the membrane [7]. However, single-drug delivery by electrospinning membranes may still be insufficient. Usually, during the first week of treatment, some patients may require a single administration of antibiotics, while others may benefit from a delayed and continuous release of osteogenic factors combined with cell-homing factors. To address these limitations, the development of dual drug delivery systems has emerged with the advancements in nanotechnology. These systems have demonstrated excellent capabilities in delivering two drugs simultaneously. For example, Gentile et al. produced electrospinning nanofibers (NFs) loaded with nano-hydroxyapatite, followed by multilayer nanoencapsulation of bio-functional peptides using layer-by-layer (LbL) methods to mimic the early events in bone healing, including the formation of a hematoma and the recruitment of inflammatory cells (neutrophils & macrophages) [8]. They also found that within a few days, mesenchymal stem cells (MSCs) began to migrate to the fracture site and differentiate. In another study, Wang et al. proposed a core-shell nanofiber membrane that had the potential to prevent infections and enhance bone growth [9].

Considering the bone tissue regeneration process, there are two essential steps. It begins with recruiting osteoblast progenitor cells into the injury site [10], followed by the need to cause and improve overall osteoblast function to accelerate bone regeneration [11]. In the past decades, the connection between the cell homing and osteogenic promotion has garnered considerable attention. Following a bone injury, the initial inflammatory response involves neutrophil infiltration into the damaged area, recruiting a second wave of inflammatory cells (e.g., monocytes, macrophages, and lymphocytes, etc.) through pro-inflammatory and chemotactic signals [12]. The subsequent secretion of cytokines and chemokines by these inflammatory cells trigger the migration and recruitment of mesenchymal stem cells (MSCs) and osteoprogenitor cells from their respective local niches to the site of injury [12]. Liu et al. have studied the differential impact of simvastatin (SIM) and stromal cell derived factor 1a on promoting bone tissue regeneration [13]. However, in their study the delivery means of the drugs lacked insight, and drug release in an uncontrolled and/or non-sequential manner. Therefore, a potential research gap might be to develop a hierarchical nanofiber membrane with a dual drug delivery system that can release cell-homing factors and osteogenic agents in a controlled and tailored manner. This membrane could potentially optimize the balance between early cell recruitment and overall osteoblast function, accelerating bone regeneration in a way that is tailored to individual patients' needs and circumstances.

In our previous research, we have successfully prepared a hierarchical polycaprolactone/gelatin (PCL/GEL) co-electrospinning membrane with the ability to deliver two different drugs in a tunable manner [14]. The PCL in the membrane indirectly regulates the degradation of GEL, which creates a tunable initial release of drugs from a hydrophilic GEL fiber and subsequent sequential release from a hydrophobic PCL fiber, resulting in a complex multifunctional copolymer-based drug delivery system. Based on this, we plan to design a co-electrospinning membrane composed of Substance P (SP)-loaded GEL fibers and SIM-loaded PCL fibers in this study, using a cell homing method to enhance cell recruitment and promote osteoblast progenitor cell differentiation. SP is a neuropeptide initially secreted by sensory nerve fibres in the periphery and is a member of the tachykinin neuropeptide family. It is bound to its receptor, neurokinin type 1 (NK-1R), which is found on numerous cell types in the body, including lymphatics, fibroblasts, vascular endothelial cells, white blood cells, and neurons [15]. A previous study has revealed that injuries have been shown to activate SP as a messenger that prompts the body's natural repair mechanisms, which in turn recruits and migrates mesenchymal stem cells (MSCs) to the damaged area [16].

SIM is a drug used to lower cholesterol and reduce the risk of cardiovascular disease. Recent studies have also shown that SIM has therapeutic benefits beyond its cholesterol-lowering effects [17,18]. Specifically, SIM has been found to promote angiogenesis, which is important for bone regeneration and tissue repair. For example, Bitto et al. claimed that SIM could increase the expression of vascular endothelial growth factor (VEGF) and promote endothelial cell migration and tube formation, leading to enhanced angiogenesis [19]. Pullisaar et al. confirmed that SIM enhanced the expression of osteoblast-related genes and the secretion of several osteogenic markers, including osteoprotegerin (OPG), vascular endothelial growth factor A (VEGFA), osteopontin (OPN), and osteocalcin (OC), in human adipose tissue-derived mesenchymal stem cells (hAD-MSCs) cultured on scaffolds with SIM compared to those without SIM [20]. These results suggest that SIM has positive effects on angiogenesis and osteogenesis, and may have potential as a therapeutic agent for tissue regeneration.

Accordingly, inspired by the structure of extracellular matrix (ECM) and the natural bone healing process, a hierarchical PCL/GEL membrane was aimed to fabricate with SP-loaded GEL as the nanofiber (easy to degrade) and SIM-loaded PCL as the microfiber (relatively difficult to degrade). The co-spinning membrane was designed to provide a sustained release for SP over two weeks. Simultaneously, the slow degradation of the PCL could allow SIM to sustain release for over a month, where it can ensure continuous osteogenic induction until the new bone is formed. The purpose of the current work as drawn in Scheme 1 was as follows: 1) to develop a bio-active membrane loaded with SIM and SP; and 2) to evaluate its biological effects on early cell recruitment and investigate the effect on angiogenesis and osteogenesis *in vitro* and *in vivo*.

2. Materials and methods

2.1. Membrane fabrication and characterization

The target membranes were prepared using the co-electrospinning method with two separate needles, as illustrated in Scheme 1 and as previously described in our work [14]. In detail, to prepare the solutions, 15 w/v% PCL and 20 w/v% GEL were dissolved in 2,2,2-Trifluoroethanol (TFEA) and a mixed solution of H_2O/TFEA (v/v = 4:1), respectively, resulting in solutions A and B. Subsequently, SIM (0.5, 1, 2.5, 5, or 10 mg/mL) and SP (100 μg/mL) were added to the PCL and GEL solutions, respectively, yielding solutions C and D. Regarding SP concentration, we chose 100 μg/mL based on a previous study that showed similar migration rates and cell viability of MSCs on the surface of materials loaded with 100 and 500 μg/mL SP after 24 h of culture [21]. So, we chose the lower concentration of 100 μg/mL to reduce material cost in our experiments. It is worth noting that all four solutions were stirred overnight until a clear and homogenized solution was obtained. The co-electrospinning process was then conducted using two syringes, each filled with either solution A or B, or solution C or D. The flow rates were set at 2 and 1 mL/h for the respective syringes. A voltage of 20 kV and a rotational speed of 300 rpm were applied during the electrospinning process. The distance between the needles and the drum collector, which was covered with an aluminum foil sheet, was maintained at 15 cm. Based on the initial electrospinning solution with/without SIM (2.5 mg/mL) and SP (100 μg/mL), the resulting samples were labeled as follows: PCL/GEL (solution A & B), PCL/GEL-sp (solution A & D), PCL-sim/GEL (solution C & B), and PCL-sim/GEL-sp (solution C & D), respectively. After the electrospinning process, all samples were vacuum-dried for 24 h to remove any residual solvent.

To evaluate the structure of the different PCL/GEL co-electrospinning membrane and their fibers size and distribution, different PCL/GEL samples were observed using scanning electron microscopy (SEM, Zeiss AURIGAFIB, Germany) at 10 kV voltage. Different membranes were placed on the SEM sample plate by conductive tape and sprayed with gold for 45 s (Leica EM ACE600). The distribution and average diameter of PCL and GEL fibers were then analyzed by measuring 100 random fibers from twelve SEM images with Image J software according to our previous study [14]. When PCL/GEL co-electrospinning was prepared using PCL15% and GEL 20%, micrometre sized fibers were confirmed to be PCL fibers, while nanoscale fibers were GEL fibers. The Fourier

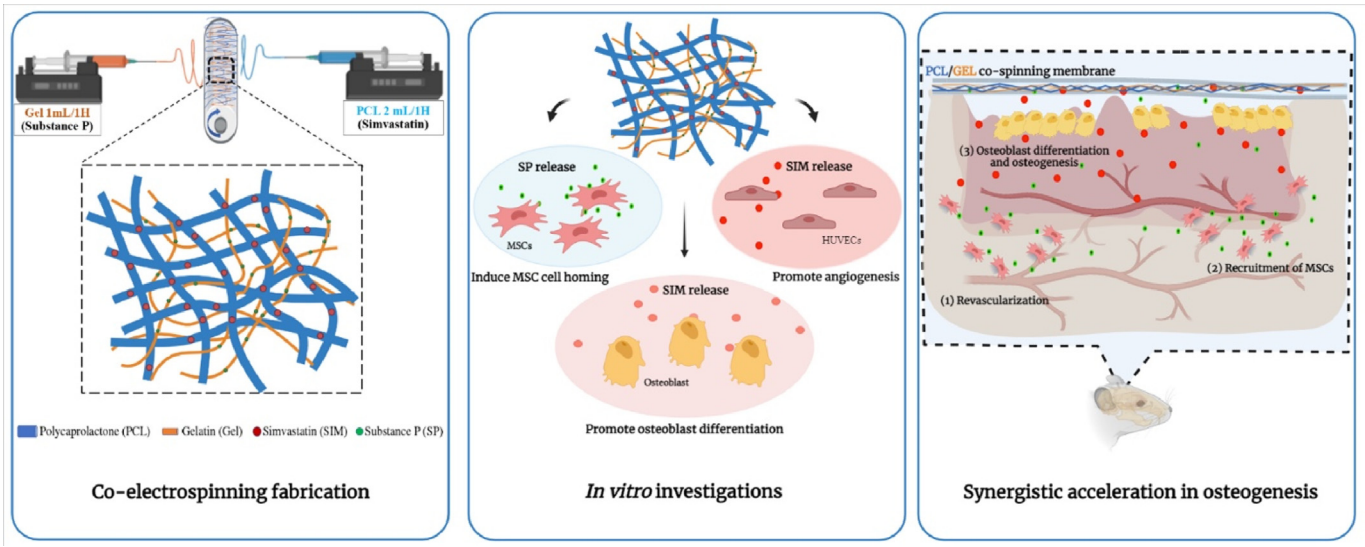

Scheme 1. Schematic illustration of the composition of co-electrospinning membrane and its biological effects on early cell recruitment, angiogenesis and osteogenesis *in vitro* and *in vivo*.

transform infrared spectroscopy (FTIR) was used to study the chemical structure of different drug-loaded films. The samples were mixed with potassium bromide (KBr) at a ratio of 1:20, compressed into sheets under 20 MPa conditions, and then analyzed by a Fourier transform infrared spectroscopy (FTIR, Thermo scientific, Nicolet 6700, USA).

2.2. In vitro drug release of SIM and SP

Before electrospinning, SIM (2.5 mg/mL) was dissolved in the TFEA solution containing PCL (15 wt%), while FITC-SP (10 μg/mL) was dissolved in the mixture solution of deionized water and TFEA (v/v = 4/1) containing GEL (20 wt%). For drug release determination, samples (50 mg) were soaked in 5 mL of phosphate-buffered saline (PBS) and incubated at 37 °C.

Firstly, to assess the release rate of SIM, 1 mL of the soaking medium was withdrawn and replaced with fresh PBS at each predefined time point (1, 6, 24, 48, 72, 144, 216, 336, 432, 504, 600, 672, 744 h). The amount of SIM in the supernatant was measured at 238 nm using a UV–Visible spectrophotometer (Thermo ScientificTM, Nanodrop 2000 and 2000c, USA) [14]. Secondly, the release of SP was measured using fluorescein isothiocyanate-labeled SP (FITC-SP), following a previously reported method [22]. The FITC-SP was loaded in GEL in PCL/GEL-sp and PCL-sim/GEL-sp membranes using the same procedures. Then, 1 mL of soaking medium was collected and replaced by new PBS at each predefined point (0.5, 1, 24, 48, 120, 168, 216, 288, 336 h). The FITC-SP was detected by recording the fluorescence intensity of emission wavelength at 540 nm and excitation wavelength at 488 nm utilizing the spectrophotometric microplate reader (Bio-Rad 680, USA) [22]. It is worth noting that the release behavior of FITC-SP was only investigated within 336 h because of the sensitivity limitation and quenching characteristics of fluorescence. Each of the release experiments was repeated four times.

Next, to determine the loading efficiency, different co-electrospinning membranes were collected from the aluminum foil, vacuum dried for 24 h at 40 °C, and then weighed one by one. The theoretical loading dose of drugs in 50 mg PCL/GEL co-electrospinning membranes was obtained by theoretical calculation: theoretical dose = total weight of the loaded drug/total weight of the co-electrospinning membrane × 50 mg. In addition, after fully dissolving the drug-loaded films (50 mg) in TFEA solution, the actual loading dose of two drugs could be directly measured. The SIM and FITC-SP were detected using UV–Visible spectrophotometer and microplate reader, respectively. The drug release percentage at different time points and the drug loading efficiency in different samples were obtained by calculating the ratio of the drug release content to the actual total dose mentioned above. Furthermore, to investigate the drug distribution of SIM and SP in the PCL/GEL co-electrospinning membranes, we utilized a confocal laser microscope (CLSM, Nikon A1, Japan). The CLSM allowed us to visualize and analyze the spatial distribution of the drugs within the membrane samples.

2.3. In vitro osteogenesis-related experiments

Before commencing the cell studies, the dried membranes were cut into squares measuring (1.5 mm × 1.5 mm) and sterilized using UV irradiation for 2 h. Each experimental group consisted of four replicate samples in all cell-related experiments. A 24-well plate was used for *in vitro* cell culture investigations, and the membrane was fixed with a sterilized custom-made titanium ring to prevent the membrane from floating. MSCs were collected from the tibia and femur of male Sprague Dawley (SD) rats and cultured in DMEM (low glucose) medium supplemented with 10% FBS and 1% penicillin-streptomycin. Every three days, all of the culture medium was discarded and replenished.

2.3.1. Cell viability

The cell viability was assessed using the Cell Counting Kit-8 assay (CCK-8), which is a widely used method for evaluating the cytotoxicity of membrane. Mesenchymal stem cells (MSCs) with an initial density of 1×10^4 cells/cm^2 were cultured on co-electrospinning membranes for 3 and 7 days. Afterward, the medium was gently discharged at the predetermined time, and then a 400 μL culture medium containing a 10% CCK-8 solution was added. After further incubation for 2 h, a new 96-well plate was filled with 200 μL of the incubated medium and transferred to record the OD value. The absorbance value was determined using a spectrophotometric microplate reader (Bio-Rad 680) at 450 nm.

2.3.2. Cell morphology

The cell morphology was investigated by staining the cell nucleus and cytoskeleton, as reported elsewhere [23]. Briefly, MSCs with a density of 4×10^3 cells/cm^2 were grown on the co-electrospinning membranes. After incubation for 2 d, the medium was discarded, and the samples were gently washed with PBS. After that, the cells were fixed using 4% paraformaldehyde for 1 h. Then, the cell nuclei were stained with 4′, 6-diamidino-2-phenylindole (DAPI) (10 min, blue-fluorescent), and the cytoskeleton was stained with Phalloidin (40 min, green-fluorescent).

Finally, the cell was observed under an inverted fluorescence microscope (FM, OLYMPUS IX81, Japan). Moreover, the cell morphology was further observed under SEM. After fixation with 4% paraformaldehyde for 1 h, the membranes were gradually dehydrated using ethanol (20, 40, 60, 80, and 100%) and then left to dry overnight. Before the SEM observation, samples were coated with platinum for 1 min to improve the conductivity.

2.3.3. Cell migration

The transwell assay was used to investigate the long-term ability of co-electrospinning membranes loaded with SP and SIM to stimulate the migration of MSCs *in vitro*. Before the experiment, the different groups were soaked in sterilized PBS and incubated at 37 °C for different times (0 and 5 d). Afterward, the pre-soaked samples were inserted into 24-well plates, and 600 μL of α-MEM medium containing a low-serum 1% FBS was added. After that, transwell chambers (pore size = 8 μm, Corning, USA) were inserted. MSCs with an initial density of 1×10^4 cells/cm^2 were cultured in upper chambers and incubated. After incubation for 12 and 24 h, the upper chamber was collected, and the migrated cells through the pores to the bottom wall were fixed by 4% paraformaldehyde and stained with 0.05% crystal violet for 10 min. The non-migrated cells on the upper side were carefully removed using a cotton swab. Finally, five separate random areas were captured using an inverted microscope (Axio Observer), and Image J software was used for quantitative analysis.

2.3.4. Alkaline phosphatase (ALP) activity

MSCs at an initial density of 1×10^4 cells/cm^2 were seeded onto different membranes for 4 and 7 d. For ALP staining to be visualized, at each predetermined time point, cells were fixed with 4% paraformaldehyde for 1 h, and then stained following the protocol provided by 5-bromo-4-chloro-3-indolyl-phosphate/nitro blue tetrazolium (BICP/NBP) Alkaline Phosphatase Color Development Kit (Beyotime, China). Finally, the stained membranes were captured using a stereoscopic microscope (NIKON, Japan). For the ALP activity assay, cells were subjected to lysis using 1% Triton X-100 in ice for 40 min. The supernatant was collected by centrifuging at 12,000 rpm for 10 min. The total protein content and ALP activity were measured using a Bicinchoninic acid assay kit (Beyotime, China) and an alkaline phosphatase assay kit (Nanjing Jiancheng Bioengineering Institution, China). The OD values for protein and ALP detection were recorded using a spectrophotometric microplate reader (Bio-Rad 680, USA) at 562 nm and 520 nm.

2.3.5. Alizarin red S staining assay

MSCs at an initial density of 1×10^4 cells/cm^2 were seeded onto different membranes for 14 and 21 d. At each time point, cells were fixed with 4% paraformaldehyde for 1 h and then stained with alizarin Red S solution for 45 min in the dark. Subsequently, the samples were washed with ddH_2O until no more stains appeared in the washing solution. Then, the samples were imaged using a stereoscopic microscope (NIKON, Japan). The stained calcium nodules were subjected to 10% cetylpyridinium chloride for 30 min for quantitative analysis. The dissolved staining solution was extracted and transferred to a new 96-well plate, and the corresponding OD values were recorded at 540 nm. Furthermore, the mineralized nodules on different membranes after 21 d were further observed by SEM.

2.3.6. Real-time PCR

To assess the expression of osteoblast-related genes [*ALP*, collagen I (*COL I*), runt-related transcription factor 2 (*Runx2*), and osteocalcin (*OCN*)], MSCs were grown on different membranes at an initial density of 2×10^4 cells/cm^2 for 7 d. Subsequently, 2 μL of the RNA was used to synthesize single-stranded cDNA through reverse transcription reactions using the PrimeScriptTMRT reagent kit (TaKaRa, Japan). The expression levels of the four target genes were then analyzed using SYBR Premix ExTM *Taq*II (TaKaRa, Japan) with specific primers listed in Table S1. The relative expression levels of the target genes were normalized to the expression of glyceraldehyde-3-phosphate dehydrogenase (GAPDH).

2.4. In vitro angiogenesis-related experiments

2.4.1. Preparation of the extract

Human umbilical endothelial cells (HUVECs) obtained from the Cell Resource Center (Chinese Academy of Sciences, China) were selected for establishing an *in vitro* angiogenesis model. The HUVECs were cultured in Dulbecco's Modified Eagle Medium (DMEM) supplemented with 10% FBS and 1% penicillin. The culture medium was refreshed every two days until the cells reached approximately 80%–90% confluency, at which point cell passage was performed. The angiogenesis-related experiments were conducted using an indirect approach. The supernatants and factors secreted from different PCL/GEL membranes were collected by immersing the samples in DMEM (1.25 cm^2/mL) at 37 °C under a 5% CO2 atmosphere for three days, following a protocol described in a previous study [24]. The extract was carefully collected and stored at −20 °C to serve as a culture medium for the HUVEC experiments.

2.4.2. Wound healing assay

HUVECs were cultured with a complete extract-added medium supplemented with 10% FBS at a density of 3×10^5 cells/cm^2, and cultured in 24 well plates until reaching about 90% confluence. A horizontal line was created at the center of each well by gently scratching the cell layer using a P10 pipette tip. The HUVECs were further incubated with extracted medium supplemented with low-serum 1% FBS. The scratched wound area was captured using a microscope (Axio Observer) at 0, 6, and 12 h after scratching. Three views of the wound area (upper, lower, and middle) were selected for image capture. The width of the scratched area was quantitatively analyzed using Image J software. The rate of wound closure was calculated as the percentage decrease in the original scratch width over time [25].

2.4.3. Tube formation

The tube formation assay was performed according to the protocol provided by another study [23]. Before cell culture, all tools were pre-cooled. Afterward, the Matrigel matrix (50 μL/well) was added to plates and incubated at 37 °C for 30 min. Subsequently, HUVECs were prepared at an initial density of 1.5×10^5 cells/cm^2 with different extract-added medium and seeded on the pre-treated Matrigel matrix plate to produce capillary-like structures. After 3 and 6 h, the HUVECs in the random areas were photographed with an inverted microscope (Axio Observer). Finally, the different parameters, including the numbers of the junction and the total length of tube formation, were quantified by the plugin tool in Image J software [26].

2.4.4. RT-qPCR assay

The expression of angiogenesis-related genes [*VEGF*, endothelial nitric oxide synthase (*eNOS*), platelet-derived growth factor (*PDGF*), transforming growth factor-beta 1 (*TGFβ1*)] was determined by RT-qPCR following the protocol as mentioned above (section 2.3.6). HUVECs were cultured at a density of 2×10^4 cells/cm^2 with extract-added mediums. After that, we used the procedure mentioned earlier to measure relative gene expression using the primers in Table S2. The relative expression levels of the target genes were normalized to the expression of GAPDH.

2.5. In vivo membrane implantation

Before conducting the animal experiments, the protocols and requirements related to animal care and use were approved by the Institutional Animal Care and Use Committee of China and the Ethics Committee of Wenzhou Medical University. A total of twenty female

Sprague Dawley (SD) rats weighing between 220 and 250 g were selected for the calvaria defect implantation study. Each rat was implanted with two different membranes to assess their performance.

The experimental procedure began by anesthetizing the SD rats through intraperitoneal injection of pentobarbital sodium (30 mg/kg). To expose the calvarium, a longitudinal incision was made in the middle of the rat's scalp following standard disinfection protocols. The surrounding soft tissue was gently dissected, and the periosteum was removed using an elevator. Bilateral defects were created on the calvarium using a trephine bur with a diameter of 5 mm, and normal saline irrigation was performed during the procedure. Next, the different membranes were implanted to cover the defects, and the incisions were closed using simple interrupted sutures. Following the surgery, the rats received daily intravenous penicillin for the first three days. After 5 or 30 days of implantation, the SD rats were sacrificed, and specimens were collected for further analysis.

2.5.1. Micro-computed tomography (Micro-CT) detection

After a 30-day period of implantation, the long-term regenerative potential of the various PCL/GEL membranes within the defect areas was assessed using Micro-computed tomography (Micro-CT) imaging. The Micro-CT scans were performed using a Skyscan1176 system (Bruker, Germany). The samples were subjected to a 360° rotation of the X-ray beam, with the following scanning parameters: 45 kV, 550 mA, and a 0.2 mm aluminium filter. The spatial resolution of the scans was set at 18 μm. To generate 3D images, the acquired scan data were reconstructed using the SCANCO software, specifically the Data Viewer module. For quantitative analysis, the SCANCO software tools, including CTVox, CTAn, and CTVol, were utilized. These tools allowed for the calculation of key parameters in the region of interest, including bone volume/total volume (BV/TV), trabecular thickness (Tb·Th), and connectivity density (Conn.Dn).

2.5.2. Histological analysis

Following an implantation period of 5 and 30 days, the collected samples were subjected to histological analysis to examine the MSC recruitment, angiogenesis, and new bone regeneration. Initially, the harvested specimens were fixed in 4% formaldehyde for three days, followed by decalcification with 10% formic acid over a 14-day period. Subsequently, the specimens were carefully extracted, gradually dehydrated in alcohol, and embedded in paraffin blocks. Sections, approximately 3–5 μm thick, were then cut from the center of the embedded pieces and used for subsequent staining procedures. The deparaffinized and rehydrated samples were blocked with 5% BSA at room temperature for 30 min.

To assess the chemotactic capability of the SP/SIM-loaded PCL/GEL membrane *in vivo* after 5 days of implantation, monoclonal antibodies targeting CD29 (mouse source; Santa Cruz Bio., China) and CD90 (rabbit source; Affinity Biosciences, China) were employed. The samples were probed with these antibodies diluted in 5% BSA and incubated overnight at 4 °C. Subsequently, the samples were washed with PBS and incubated with Cy3-conjugated Donkey Anti-Mouse IgG and FITC-conjugated donkey anti-rabbit IgG antibodies (Sangon, China) for 1 h. Nuclei of somatic cells were stained with Hoechst 33,258. Confocal laser scanning microscopy (CLSM, TCS SP5, Leica, Germany) was used to capture images of the stained samples. Additionally, the samples were subjected to CD34 and von Willebrand Factor (vWF) immunohistochemical staining to assess neovascularization density. Hematoxylin/eosin stain (H&E) and Masson's trichrome staining were performed to evaluate the histological characteristics of new bone regeneration after 30 days of implantation.

2.6. Statistical analysis

The data were presented as mean ± standard deviation. Data analysis (GraphPad Software, USA) was tested by One-way ANOVA followed by Tukey's multiple comparison test to evaluate the differences between the four groups unless otherwise stated. P^* <0.05 and P^{**} <0.01 were defined as statistically significant.

3. Results

3.1. Surface characterization

The surface characterization of different membranes was investigated in terms of morphology and chemical composition. The morphology was first studied using SEM at various magnifications (Fig. 1A). At low magnification, the PCL and GEL fibers showed a hierarchical, uniform, and randomly oriented micro-nanofibrous structure. While, at high magnification, both fibers were smooth, continuous, interconnected, and had no bead-shaped defects. Furthermore, the quantitative analysis of fibre diameter is displayed in Fig. 1B, we can find that the GEL fibre had consistency in fibre size in all groups, with average diameters of 0.32 ± 0.15 μm (consistent with the size of our previous study [14]), indicating that the addition of SP has a negligible impact on the GEL fibre size. On the contrary, adding SIM considerably impacted PCL fibre diameter, where it decreased from about 1.5 μm in PCL/GEL and PCL/GEL-sp to approximately 1.3 μm in PCL-sim/GEL and PCL-sim/GEL-sp membranes.

Next, the FTIR spectra were carried out to investigate the chemical composition of the target material, including two single fibers (PCL, GEL), SIM drug, and four co-electrospinning membranes (PCL/GEL, PCL/GEL-sp, PCL-sim/GEL, PCL-sim/GEL-sp). As demonstrated in Fig. 1C, for the GEL fibers, strong peaks appeared at approximately 1652 cm^{-1} and 1540 cm^{-1}, which is attributed to amide I (stretching vibration of C═O) and amide II (stretching vibrate of C–N and coupling of bending vibrates of N–H), respectively. The infrared spectra of PCL single fibers were defined by stretching modes at 2869 cm^{-1} (symmetric CH_2 stretching), 1734 cm^{-1} (C═O), and 1170 cm^{-1} (C–*O*–C). While, SIM characteristic peaks were observed in a specific band at 1692 cm^{-1} (C═O) and 1272 cm^{-1} (C–*O*–C). The spectra of these drug-loaded PCL/GEL co-electrospinning membranes were identical to those of single polymers or/and drugs, without distinctive features. This similarity could be attributed to the comparatively tiny amounts of loaded drugs that might have been shifted or replaced by the peaks of the polymers, resulting in this effect [27].

3.1.1. SP and SIM drugs loading and release

During the electrospinning process, the loading efficiency of drugs depends on their solubility in the polymer solution. If the drug completely dissolves and does not volatilize, a loading efficiency of 100% can be achieved [28,29]. The simplest method for incorporating drugs into nanofibers is to dissolve the drugs and polymer in the same solvent and electrospin them together. This method typically results in high drug-loading efficiency [30]. In our study, the solubility of SIM/PCL in TFEA and the solubility of GEL/SP in water enabled the formation of transparent polymer solutions containing the drugs. This suggests that the drugs were uniformly dispersed in the polymer solution at a molecular level. As a result, we achieved high loading efficiencies of 98.7% for SIM and 98.4% for SP, respectively. The high encapsulation efficiency observed can be attributed to the large surface area of the nanofibers and the absence of drug loss during the preparation process [31]. These factors collectively contribute to the successful incorporation of the drugs into the nanofibers and the high loading efficiency observed in our study.

Furthermore, in order to provide additional evidence of fiber type and drug distribution within the fiber, we used FITC-SP and rhodamine B (RB) to label GEL (green) and PCL (red) fibers, respectively. Because SIM is difficult to achieve fluorescent labeling, it is necessary to use the model substance (RB) to study its distribution in PCL fibers. As demonstrated in Fig. S2, it was discovered that both drugs were evenly distributed in the corresponding fibers. It is important to highlight that the two different colors representing the microscale PCL and nanoscale GEL fibers in the figures appear to overlap each other. This can be observed by examining the SEM images (Fig. 1A), where the PCL and GEL fibers can be seen

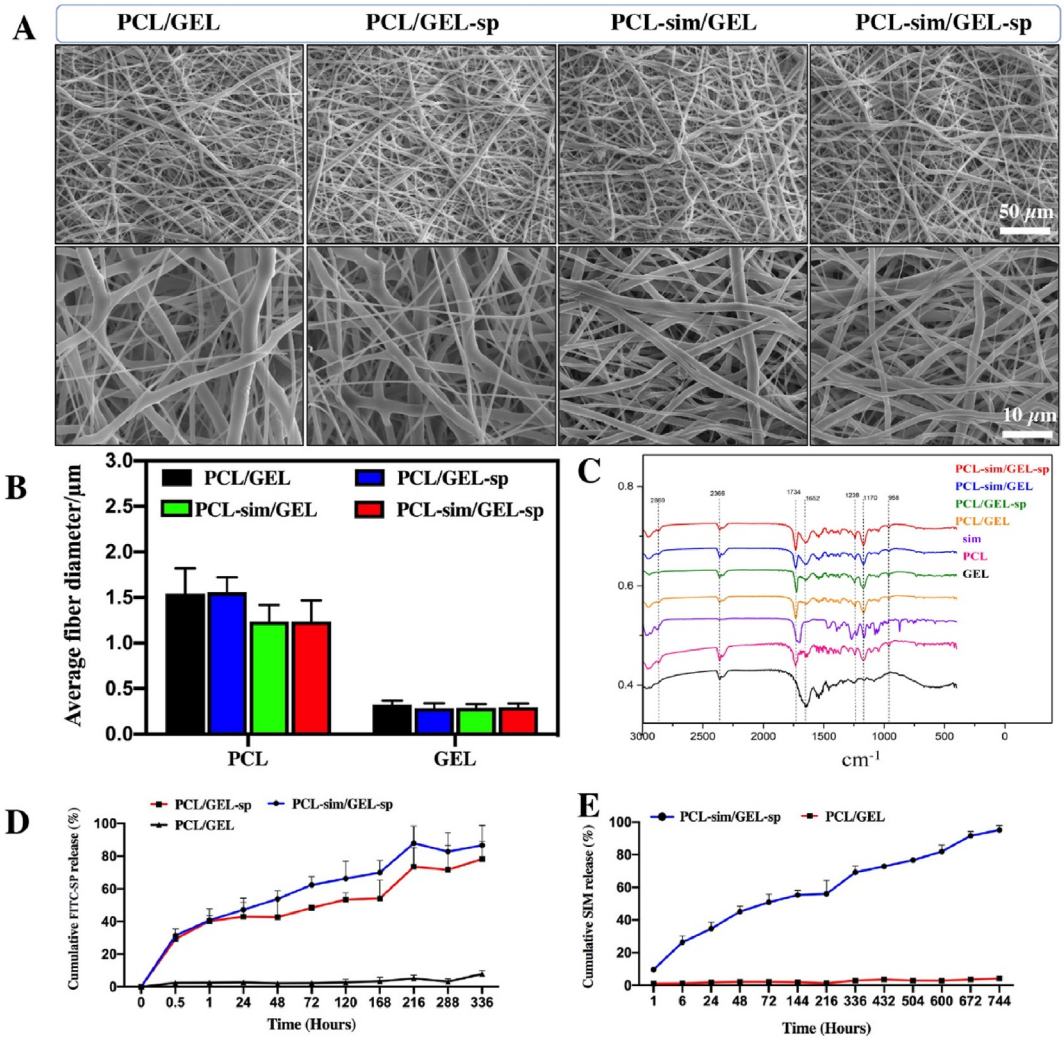

Fig. 1. (A) SEM images of different co-electrospinning membranes at various magnifications; (B) the average fiber diameter of GEL and PCL fibers according to SEM data; (C) FTIR spectra of single fibers (PCL, GEL), free drugs Sim and co-electrospinning films (PCL/GEL, PCL/GEL-sp, PCL-sim/GEL, PCL-Sim/GEL-sp); (D) releasing curve of FITC-SP from PCL/GEL, PCL/GEL-sp, and PCL-Sim/GEL-sp membranes; and (E) releasing curve of SIM from PCL/GEL and PCL-Sim/GEL-sp membranes.

overlapping, as confirmed in our previous research [14]. In certain areas, it is evident that the GEL fiber is partially covered by the PCL fiber, indicating a degree of interlayering and intertwining between the two types of fibers.

The release of SP from PCL/GEL-sp and PCL-sim/GEL-sp samples was assessed by observing the fluorescence intensity. As illustrated in Fig. 1D, we could see an initial fast SP release from GEL fibre in both groups, with approximately 43.5% of the drug being released on the first day. While in the following time, the SP released from PCL/GEL-sp and PCL-sim/GEL-sp membranes exhibited a sluggish and sustained release rate, dependent on the size and amount of PCL fibre in the membrane. Notably, after two days, the SP released from PCL/GEL-sp group was found to decrease by almost 12% in all-time points compared to PCL-sim/GEL-sp group. This inconsistency in controlling the drug release curve may be due to PCL fibre size changes after loading SIM, as mentioned in section 3.1. Furthermore, as demonstrated in Fig. 1E, the release of the SIM showed an initial rapid release rate within the first two days of incubation, followed by a slowly continued curve over one month.

It is worth noting that in our study, we observed that GEL fiber exhibited inherent fluorescence properties due to its degradation. Our results revealed that the accumulated fluorescence from the GEL component accounted for approximately 7% of the total drug fluorescence, as demonstrated in Fig. 1D. Similarly, the total accumulated detection of ultraviolet absorption interference at 280 nm from GEL was approximately 4% of the total ultraviolet absorption, as demonstrated in Fig. 1E. These findings indicate that the release behavior of the drugs in Fig. 1D and E is primarily attributed to the drug components rather than the degradation of the GEL itself. The small contribution of GEL fluorescence or ultraviolet absorption interference to the overall drug release confirms that the drug-loaded fibers dominate the release profiles observed in the study. Therefore, we can conclude that the release curves presented in Fig. 1D and E primarily reflect the release behavior of the drugs and are not significantly influenced by the degradation of the GEL component.

Based on these results, the PCL-sim/GEL-sp co-electrospinning membrane demonstrated the ability to deliver SP (loaded in GEL) to the bone microenvironment at a very fast and sustained rate during the critical first stage of bone healing. Meanwhile, SIM (loaded in PCL) was released in a relatively slow and sustained manner, ensuring continuous osteogenic induction during bone healing.

3.2. Membrane cytocompatibility

To assess the cytocompatibility of the PCL/GEL co-electrospinning membranes, we evaluated the cell morphology and viability of MSCs cultured on different membranes. Firstly, we determined the appropriate

concentration of SIM by loading various concentrations (0.5, 1, 2.5, 5, and 10 mg/mL) into PCL fibers in the PCL/GEL co-electrospinning membrane to evaluate their cytocompatibility. We found that higher concentrations of SIM (5 and 10 mg/mL) caused significant cytotoxicity and inhibited cell viability, while lower concentrations ranging from 0.5 to 2.5 mg/mL had no significant effect on cell proliferation, as shown in Fig. S1. Based on these results, we selected 2.5 mg/mL as the optimal concentration for our experiments.

After screening the appropriate concentration of SIM, we further examined the cytocompatibility of SP/SIM-loaded PCL/GEL samples. As demonstrated in Fig. 2A, from the fluorescence and SEM images, it was clear that the cells in PCL/GEL and PCL/GEL-sp groups showed elongated and irregular shapes. Notably, the MSCs grown on PCL-sim/GEL and PCL-sim/GEL-sp membranes (especially the latter) presented a larger spreading area and more pseudopodia. The quantitative analyses of the relative cell area (Fig. 2B) showed a similar trend to the fluorescence and SEM images. Next, from the cck-8 results in Fig. 2C, it can be noticed that four electrospinning groups had no toxicity at both 3 and 7 d. However, the tissue culture polystyrene (TCPS, blank group) group showed a significant increase in cell viability compared to the PCL/GEL-Sp and PCL-SIM/GEL-Sp groups with significant values ($p < 0.05$ or 0.01) after 3 d. With an extension of culture time to 7 d, MSCs cultured on all groups proliferated at the same rate with no significant difference.

3.3. *In vitro* MSC migration

Transwell migration assay was used to study the capability of different membranes to induce MSC migration *in vitro*, as represented in Fig. 3A. From Fig. 3B, it is intelligible that the three groups (PCL-sim/GEL, PCL/GEL-sp, and PCL-sim/GEL-sp) had distinct effects on promoting the migration of MSCs from the upper chamber to the lower chamber in varying degrees, which was related to the incubation time and the samples pre-soak duration.

Furthermore, the cell count results (Fig. 3C) displayed that when the

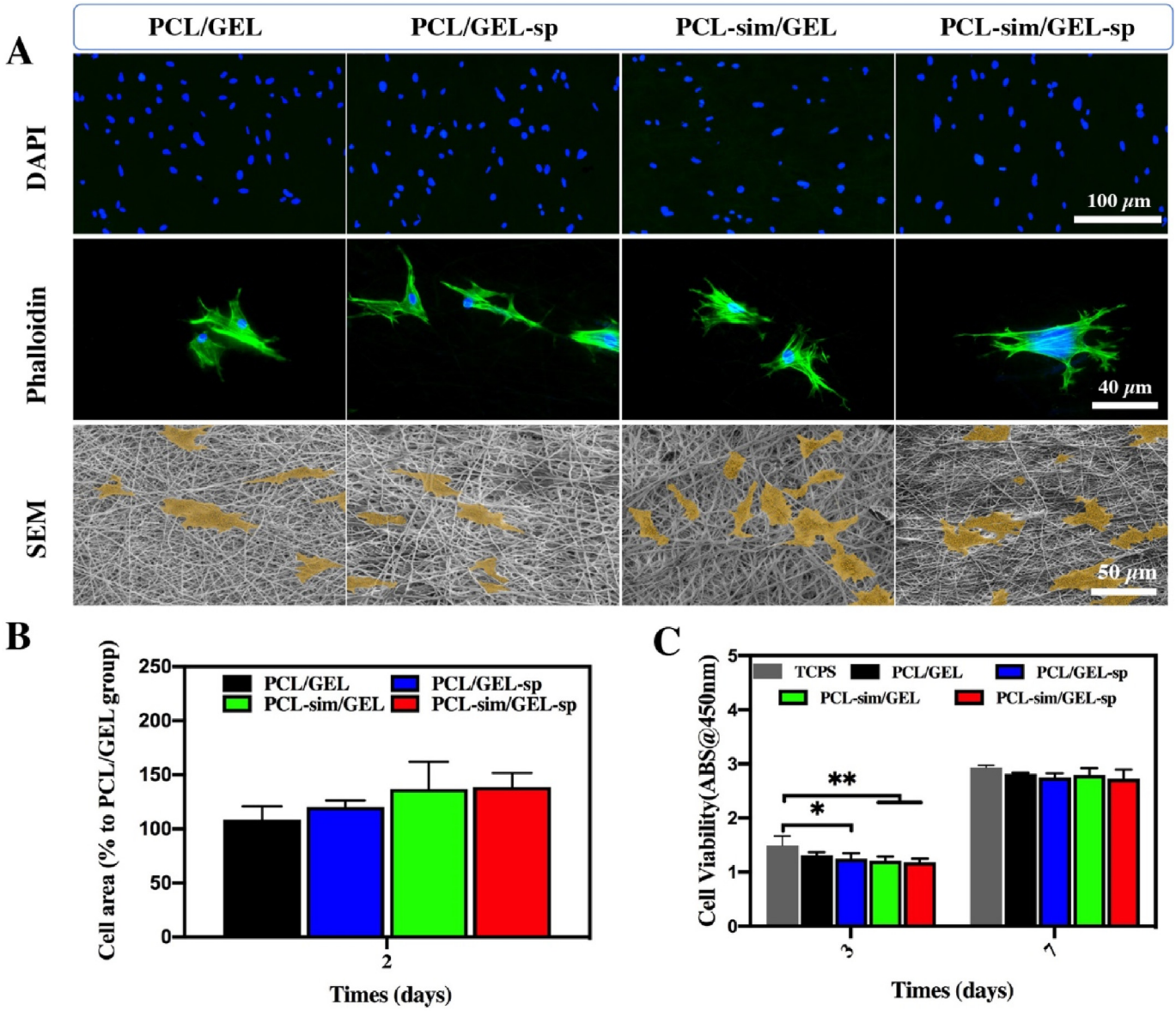

Fig. 2. Cytocompatibility of the co-electrospinning membranes. (A) Representative nucleus/cytoskeleton staining and SEM images of MSCs on different membranes after 2 d. Cell nuclei and cytoskeleton were stained by Hoechst33258 (blue) and Phalloidin (green), respectively; (B) average cell area obtained from the above fluorescent staining images; (C) cell viability evaluated by CCK-8 assay, $*p < 0.05$, $**p < 0.01$. (For interpretation of the references to color in this figure legend, the reader is referred to the Web version of this article.)

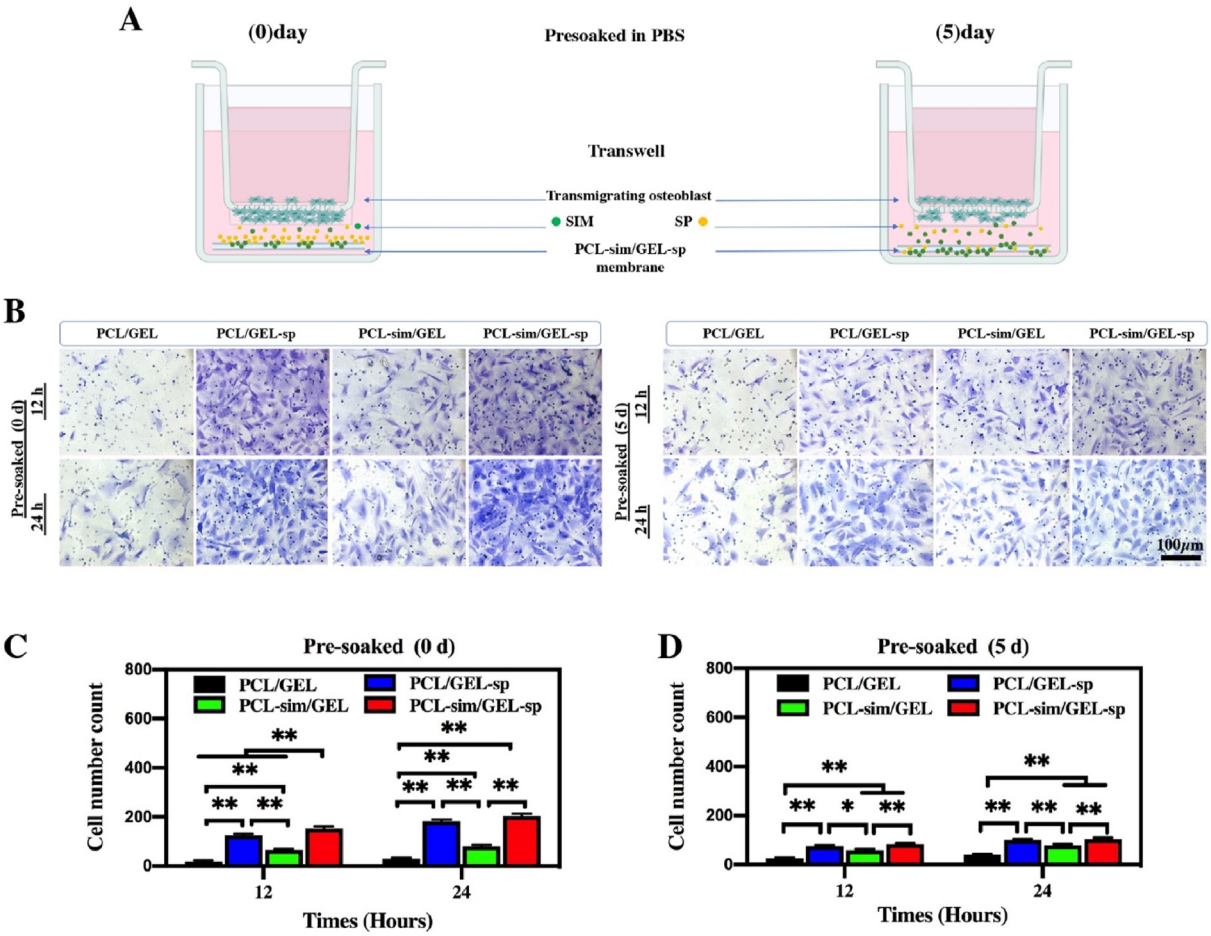

Fig. 3. Investigation of MSC migration properties by transwell assay. (A) Scheme of MSC migration by transwell assay; (B) staining images of migrated cells after culturing for 12 h and 24 h on different membranes presoaked with PBS solution for 0 and 5 d; (C) quantitative analysis of migrated cells in presoaked (0 d) test; and (D) quantitative analysis of migrated cells in presoaked (5 d) test, $*p < 0.05$, $**p < 0.01$.

pre-soaked (0 d) samples were used for the experiment, the number of migrating cells in the other three groups (especially PCL/GEL-sp and PCL-sim/GEL-sp) was significantly higher in comparison with the PCL/GEL group ($p < 0.01$). A similar trend was also observed in the pre-soaked (5 d) groups (Fig. 3D). Meanwhile, with the increase in culture time (12–24 h), the number of migrating cells in each group increased slightly. These results have important implications for developing a concept of how the sustained release of SP and delivering SIM at an appropriate concentration from the PCL/GEL co-electrospinning membrane could significantly promote MSCs migration.

3.4. *In vitro osteogenic differentiation*

A series of osteogenic-related tests were performed on MSCs cultured on different membranes, including staining, ALP activity, ALP/alizarin red staining, and RT-PCR to determine their ability to promote osteogenesis. Firstly, looking at Fig. 4A, it is apparent that the PCL-sim/GEL and PCL-sim/GEL-sp groups exhibited significantly more ALP-positive cells than the other two groups after 4 and 7 d. Furthermore, the results were obtained from the quantitative analysis of ALP activity, as shown in Fig. 4B. It is clear that the ALP activity on the 4th day was increased in the PCL-sim/GEL and PCL-sim/GEL-sp groups compared with the PCL/GEL and PCL/GEL-sp groups, with a significant difference ($p < 0.05$ or 0.01).

After 7 d of incubation, the ALP activity also showed a similar trend, and these values in PCL-sim/GEL and PCL-sim/GEL-sp groups were well over twice as high as those in other groups ($p < 0.01$). It indicates that the SIM-loaded membranes had a significant impact on improving osteogenic differentiation.

Next, the mineralization level was investigated by detecting the calcium nodules formation using alizarin red staining. SEM was further observed as an important marker for the later stage of osteoblast differentiation. As shown in Fig. 4C, after 14 and 21 d of induction, calcium nodules with wider distribution and deeper staining intensity were noticed in the PCL-sim/GEL and PCL-sim/GEL-sp samples. In comparison, no differences between the control group and PCL/GEL-sp were noticed. In fact, after 21 d, PCL/GEL-sp showed a negligible increase in the intensity and distribution of alizarin stain. Moreover, after incubation for 21 d, the calcium nodules amount was detected by SEM and shown in Fig. 4D. The high and low magnification SEM photos suggest that PCL-sim/GEL and PCL-sim/GEL-sp membranes had a superior ability to stimulate more mineralized nodule formation (red arrows). Furthermore, the quantitative analysis (Fig. 4E) shows that the mineralization level of the PCL-sim/GEL and PCL-sim/GEL-sp groups was significantly higher ($p < 0.01$) in comparison with the other two groups.

Finally, the qRT-PCR assay was employed to further explore osteogenic differentiation at the gene level. As can be seen from the data in Fig. 4F, the MSCs of the PCL-sim/GE and PCL-sim/GEL-sp groups showed significantly higher expression of COL I, Runx2, and OCN compared with the other two groups ($p < 0.05$ or 0.01). For these three genes, there was a negligible difference between the two groups (PCL-sim/GE and PCL-sim/GEL-sp). Moreover, PCL-sim/GEL-sp displayed the highest expression of the ALP gene among the four groups. PCL-sim/GEL also substantially enhanced the ALP expression compared with the PCL/GEL

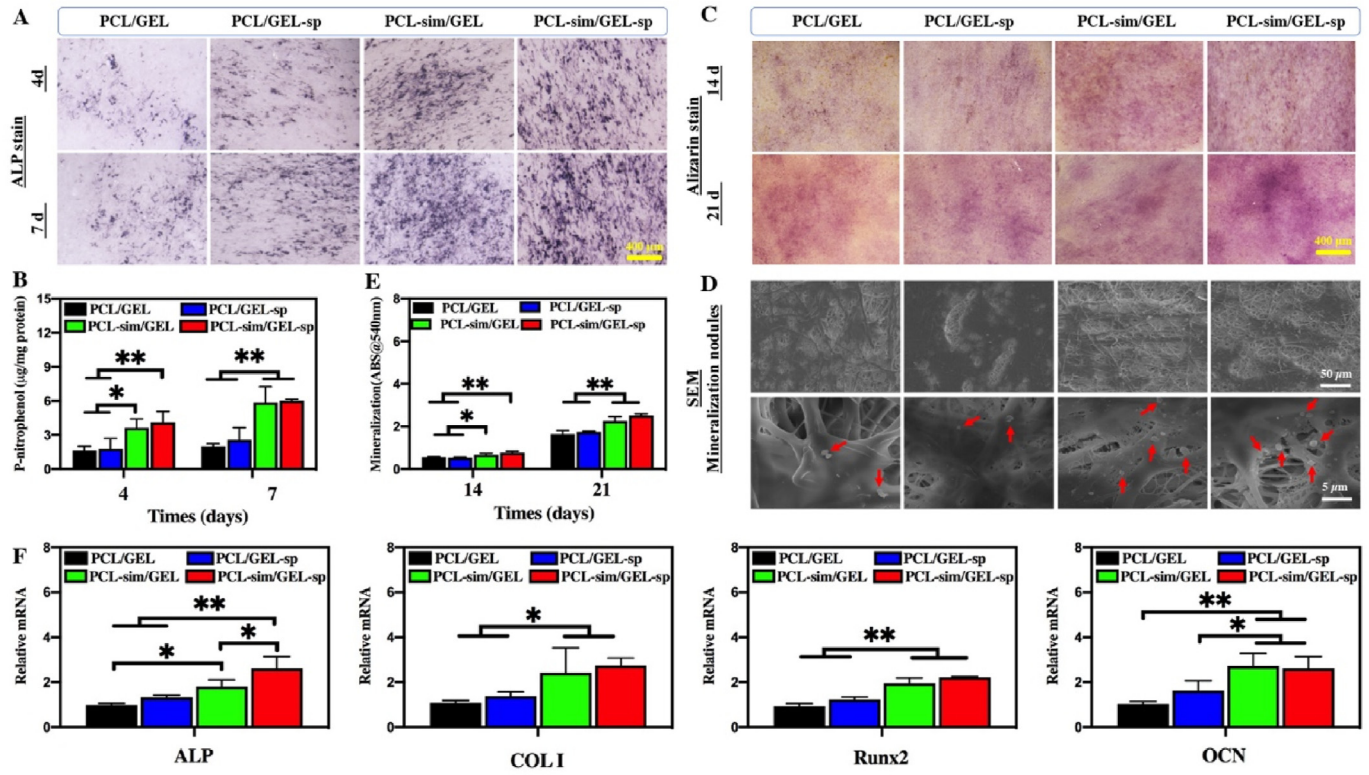

Fig. 4. Study on osteogenic differentiation of MSCs on different co-electrospinning membranes. (A) ALP staining images of MSCs cultured for 4 and 7 d; (B) quantification analysis of ALP activity; (C) Alizarin staining images of MSCs cultured for 14 and 21 d; (D) SEM images of mineralized nodules produced by MSCs after 21 d (red arrows refer to the formed mineralized nodules); (E) quantification analysis of Alizarin red stain; (F) expression of some osteogenic genes (Runx2, ALP, Col I, and OCN) after 7 d, $*p < 0.05$, $**p < 0.01$. (For interpretation of the references to color in this figure legend, the reader is referred to the Web version of this article.)

group ($p < 0.05$), with no notable difference with PCL/GEL-sp. These findings demonstrate that the sustained and synergistic effects of SP and SIM secreted from the co-electrospinning membrane could play a crucial role in promoting osteogenic differentiation at the early and late stages.

3.5. In vitro angiogenesis investigation

Angiogenesis effects of PCL-sim/GEL-sp membrane were investigated indirectly by using the secreted factors in the extraction medium to act as a stimulator on HUVECs. Angiogenesis-related assays included wound healing, tube formation, and gene expression, which were thoroughly examined and shown in Fig. 5. Firstly, the results obtained from the scratch assay were displayed in Fig. 5A. It can be found that, at 0 h, a scratch in a straight line was made, leaving a gap area with the same width in each well. Then, after further incubating for 6 and 12 h, the gap width became narrower or completely closed by the migrated cells, concerning the presence of bioactive components (SP or/and SIM) and the incubation time. Moreover, in comparison to the PCL/GEL group, the quantitative analysis confirmed that the three groups (PCL-sim/GEL, PCL/GEL-sp, and PCL-sim/GEL-sp) had a superior ability to improve the HUVEC migration (Fig. 5B). Especially, PCL-sim/GEL-sp showed the best ability to stimulate cell migration ($p < 0.05$ or 0.01).

Secondly, it can be seen from Fig. 5C that after 3 and 6 h, the primary capillary-like network structure was formed by the cell arrangement, which was obviously in PCL-sim/GEL and PCL-sim/GEL-sp groups. In contrast, only a few indistinguishable tubes were noticed in PCL-/GEL and PCL-/GEL-sp groups. Furthermore, the quantitative results of the tube length and junction were shown in Fig. 5D and E. PCL-sim/GEL, and PCL-sim/GEL-sp groups had the highest number of junctions (118 ± 7 and 127 ± 6 at 6 h, respectively), which was significantly higher ($p < 0.01$) than other groups (PCL/GEL: 80 ± 5; PCL/GEL-sp: 88 ± 3). Moreover, we also discovered that the mean tube length of PCL-sim/GEL and PCL-sim/GEL-sp was in the majority compared to PCL/GEL and PCL/GEL-sp groups, with a significant p-value ($p < 0.01$). To be precise, the mean tube length of the PCL-sim/GEL-sp group was 3401 ± 507 μm at 3 h and 5742 ± 370 μm at 6 h.

Finally, to further confirm and understand how the extracts from PCL-sim/GEL-sp promoted angiogenesis, we analyzed the gene expressions of *VEGF*, *eNOS*, *PDGF*, and *TGFβ1* using RT-qPCR. As demonstrated in Fig. 5F, it is clear that the target genes in the PCL-sim/GEL-sp group was accounted for the highest level in comparison to other groups ($p < 0.01$). Also, there was a significant increase in the levels of the genes in PCL-sim/GEL and PCL/GEL-sp compared to the PCL/GEL group ($p < 0.01$). Interestingly, compared with the PCL-sim/GEL group, the TGFβ1 gene expression in the PCL/GEL-sp group was increased, with a significant p-value ($p < 0.01$). Overall, these findings clearly indicate that the synergistic effect of SP and SIM played a critical and significant role in improving the HUVECs migration and angiogenesis.

3.6. In vivo cell migration

To further confirm and determine whether SP or/and SIM-loaded membranes could improve the migration potentiality of MSCs *in vivo*, we used double immunofluorescence labeling to detect the number and distribution of MSCs around the co-electrospinning membranes after five days of implantation. A closer inspection of the images (Fig. 6A) shows that in the PCL/GEL-sp and PCL-sim/GEL-sp groups, there was an increasing trend of CD29/CD90 positive cells ($CD29^+/CD90^+$) compared with the PCL/GEL and PCL-sim/GEL groups. Furthermore, the quantitative analysis of the $CD29^+/CD90^+$ displayed a similar trend as the immunofluorescence images. It can be seen from the data (Fig. 6B & C) that the PCL-sim/GEL-sp group had significantly more positive cells than

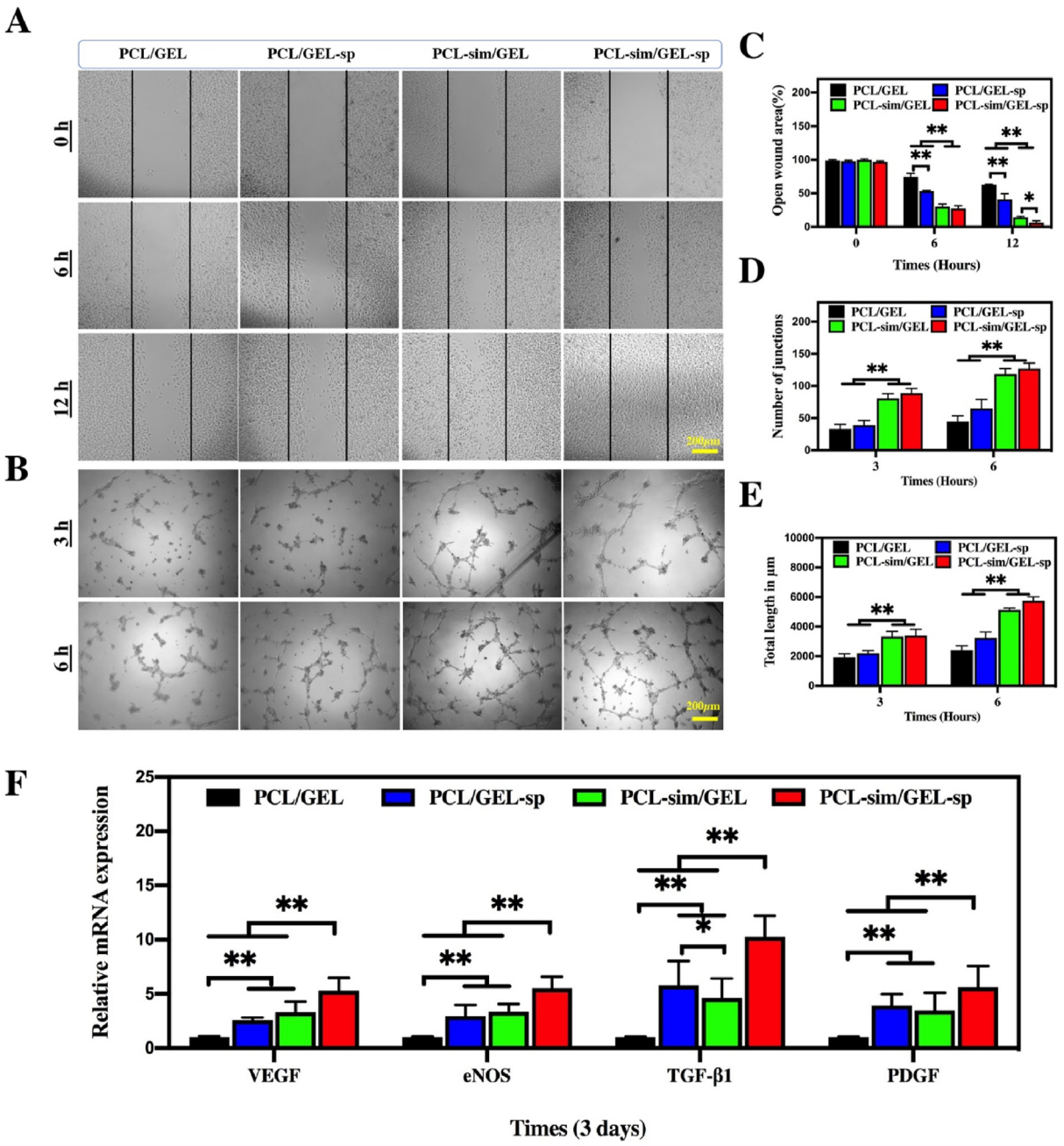

Fig. 5. Evaluation of different co-electrospinning membrane extracts on angiogenesis of HUVECs. (A) The migration images of HUVECs after culturing for 0, 6, and 12 h; (B) Images of endothelial network formation in HUVECs after incubation for 3 and 6 h; (C) quantitative analysis of the migration areas according to the above migration images; (D) the number of junctions and (E) total length per high power field (HPF) obtained from the above network images; (F) expression of some angiogenesis genes (VEGF, eNOS, TGFβ1, and PDGF) after 3 d, $*p < 0.05$, $**p < 0.01$.

the PCL/GEL and PCL-sim/GEL groups, with approximately 17.3 (PCL/GEL), 18.4 (PCL-sim/GEL), 24.8 (PCL/GEL-sp), and 27.1 (CL-sim/GEL-sp) per view field for $CD29^{+}/CD90^{+}$ cells, respectively. These findings indicated that the SP-loaded membranes have a superior ability to improve early MSC migration *in vivo*.

3.7. In vivo blood vessels formation

It is well known that vWF, as a blood glycoprotein factor, is expressed by endothelial cells and megakaryocytes, and plays a role in mediating hemostasis, especially platelet adhesion. In addition, hematopoietic marker CD34 is also highly expressed by endothelial cells. They are considered as most well-known markers for assessing the condition of revascularization *in vivo*. Therefore, immunohistochemical staining of the abovementioned factors was used to confirm the potential ability of SP or/and SIM-loaded PCL/GEL membranes to improve the new blood vessel formation *in vivo*. Looking at Fig. 7A and B), it is apparent that both PCL-sim/GEL and PCL-sim/GEL-sp groups had a superior ability to enhance early angiogenesis in the defect area after 5 d of membrane implantation. The quantitative analysis data (Fig. 7C & D) further confirmed a clear trend in the increasing number of positive blood vessels in PCL-sim/GEL and PCL-sim/GEL-sp groups compared with the PCL/GEL and PCL-sim/GEL groups. As shown in Fig. 7C, the density of $CD34^{+}$ vessels in the PCL/GEL and PCL/GEL-sp group was in the minority, with nearly 0.7 ± 0.2 and 0.8 ± 0.1 per view field, respectively. By contrast, a higher density of $CD34^{+}$ vessels were found in PCL-sim/GEL and PCL-

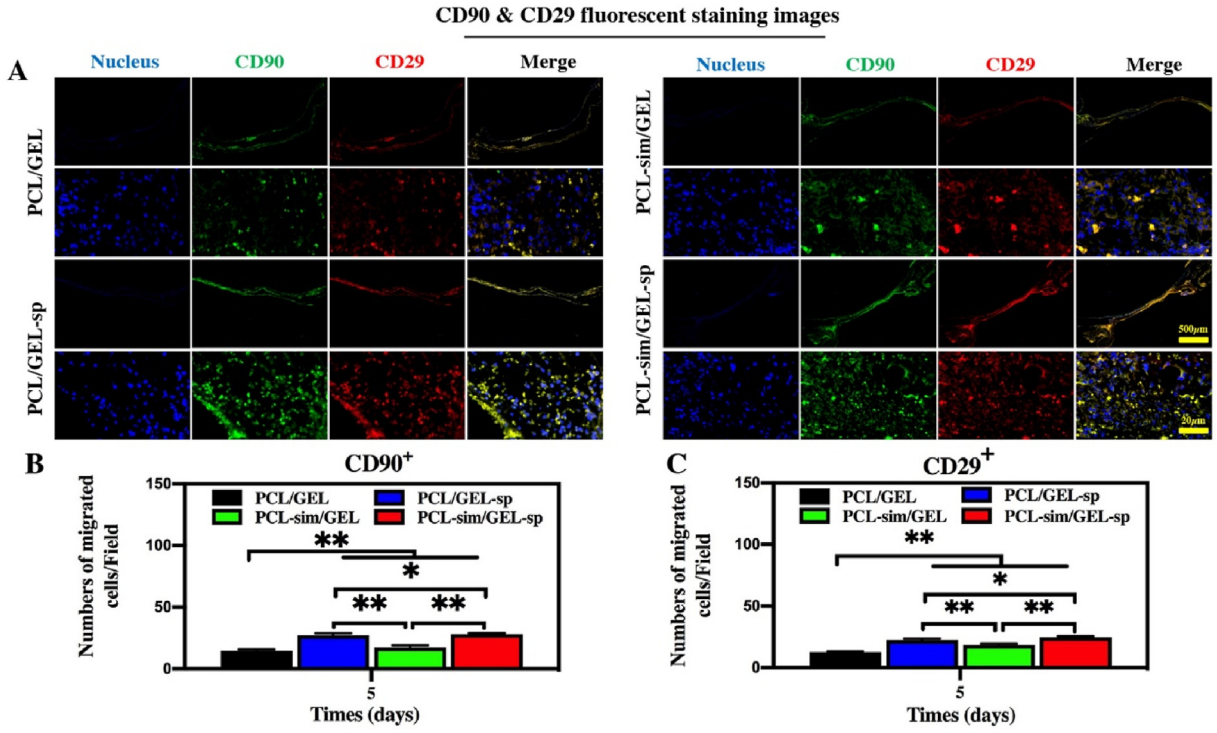

Fig. 6. Analysis of MSCs homing after five days of membrane implantation *in vivo*. (A) Immunofluorescence images of $CD29^+/CD90^+$ double-positive cells in different samples; quantitative analysis of (B) $CD29^+$ and (C) $CD90^+$ positive cells in different samples, $*p < 0.05$, $**p < 0.01$.

sim/GEL-sp groups, with approximately 1.0 ± 0.2 and 1.1 ± 0.3 per view field, respectively. Likewise, as can be seen in Fig. 7D, the density of vWF^+ vessels per view field was 1.9 ± 0.3 in the PCL-sim/GEL-sp group, with a clear significant difference ($p < 0.01$) compared to the PCL/GEL and PCL/GEL-sp groups. Notably, there was a negligible decrease in the density of vWF^+ vessels in the PCL-sim/GEL group, with 1.3 ± 0.2 per view field. These findings indicated that both PCL-sim/GEL and PCL-sim/GEL-sp membranes have an excellent ability to improve revascularization *in vivo*.

3.8. In vivo osteogenic performance

To investigate the potential ability of PCL-sim/GEL-sp membrane to accelerate a new bone reconstruction in the damaged area, the samples were scanned using a micro-CT after 4 weeks of membrane implantation. From Fig. 8A, it is observed that the scanned areas of the PCL/GEL and PCL/GEL-sp groups had weak healing ability. Only tiny and unconnected high-density spots were observed. In contrast, the healing ability of the PCL-sim/GEL group was enhanced. The scanned area exhibited that the small landmasses of new bone nodules formed in the center and along the edges of the defect. Interestingly, the PCL-sim/GEL-sp group showed the most excellent ability in bone reformation within the defect. New bone tissues with higher bone density were clearly distributed over the entire bone defect area. Further analysis (Fig. 8B & D) of the BV/TV, Tb·Th and Conn-Dens levels also showed an increasing trend in the PCL-sim/GEL-sp group with a significant difference compared to PCL/GEL and PCL/GEL-sp groups ($p < 0.01$).

H&E and Masson's trichrome staining were further carried out to estimate the effectiveness of the PCL-sim/GEL-sp membrane in accelerating bone regeneration. The H&E staining images (Fig. 9A) provided a view of the various tissues in the implantation area, where the new bone tissue presents dense dark red staining.

In Masson's trichrome stain pictures (Fig. 9B), the calcified bone with multi collagen fibers appeared in blue, while the other granulation tissues or red blood cells are dark red. High magnification histological images showed that a bone matrix with a considerable amount was conclusively demonstrated in the PCL-sim/GEL-sp membrane group, which provided significant evidence for bone regeneration one-month post-implantation. Some Haversian canals could also be found in PCL-sim/GEL-sp group, which is distributed in some middle space of the new bone formed, with an average diameter between 75 and 300 μm. By contrast, the implantation area in the PCL/GEL sample was packed with loose soft granulation growing into the implantation area, which prevents new bone formation. In addition, the PCL/GEL membrane material has been degraded to various degrees during the reconstruction process. Accordingly, inconsistently white spots were observed in histological sections.

4. Discussion

The process of natural bone formation is closely reflected in the process of bone regeneration after bone injury, including the initial inflammatory stage, the subsequent remodeling stage, and so on. These phases are interrelated and must occur one after another [32]. However, despite the complexity and difficulty of mimicking the natural healing process, this complexity has driven many researchers to design a biomaterials scaffold as a promising strategy to simulate these healing events. Therefore, a biomaterial scaffold that could improve early cell migration and blood vessel formation, followed by a continuous osteogenic induction, would be a good alternative. Accordingly, inspired by the structure of ECM and the natural bone healing process, in this study, a hierarchical PCL/GEL membrane was successfully fabricated with SP-loaded GEL as the nanofiber and partially protected by the SIM-loaded PCL as the microfiber. The co-electrospinning membrane was designed to provide a rapid initial release in the first two days, followed by a slow and sustained release for two weeks of SP-loaded GEL nanofiber to enhance the MSC recruitment to the injury site. At the same time, the slow degradation of PCL microfiber could provide controlled and sustained

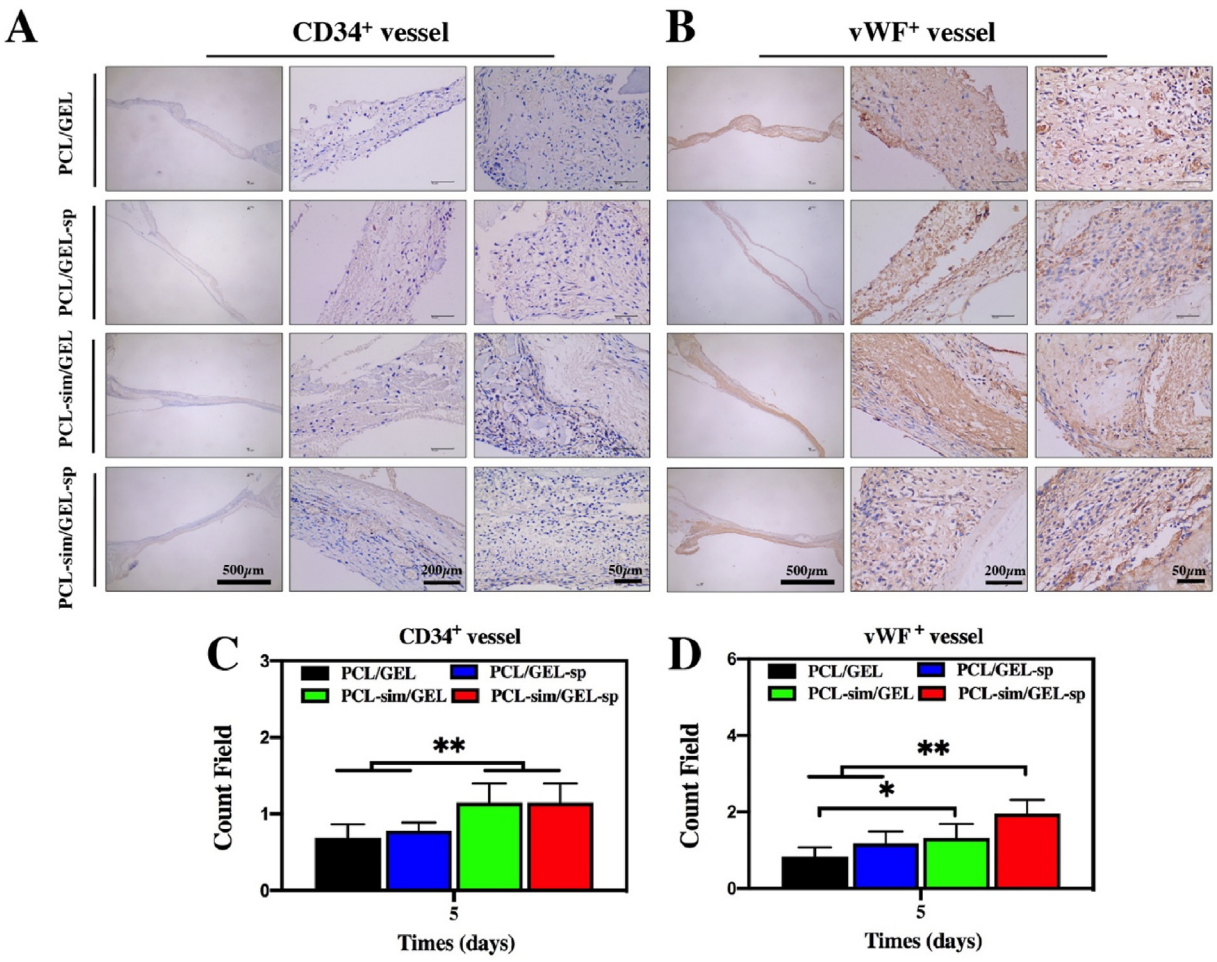

Fig. 7. Histopathological analysis of vascularization *in vivo* five days post-implantation. Immunohistochemical staining for (A) CD34 and (B) vWF in different groups; quantitative analysis of (C) $CD34^{+}$ and (D) vWF^{+} positive vessel density, $*p < 0.05$, $**p < 0.01$.

release of SIM for up to one month. It could significantly improve revascularization and continuous osteogenic induction until the new bone was formed.

The strong interaction between the fiber and water can play a critical role in the release profile of drugs loaded on the fibers, resulting in a more intense burst release. In our previous study, we found that the water absorption resistance of the PCL/GEL co-electrospinning membrane became stronger as the amount and concentration of PCL increased [14]. This indicated that as the amount of PCL increased, the hydrophobicity of the membrane also increased, resulting in slower water absorption and prolonged drug release. Moreover, the strong intra-fiber interaction of PCL repelled water and prevented direct contact between water and GEL, thereby delaying GEL degradation and initial drug release [14]. These findings combined with the drugs release results (Fig. 1D & E) suggest that PCL-sim/GEL-sp co-electrospinning membranes have good water interaction and could serve as complex multifunctional co-polymers-based drug delivery systems with tunable release profiles.

Another important consideration for the development of an ideal guided tissue regeneration membrane is its mechanical stability and integrity. The mechanical properties of the membrane play a crucial role in ensuring its ability to resist mechanical forces throughout the surgical procedure and the bone tissue regeneration process. As indicated by a previous study, bone tissue regeneration will take up to 4–6 weeks, and during this time, the GTR membrane must be able to maintain its structural integrity to prevent unwanted cell migration and facilitate a smooth bone regeneration process [33]. Our previous research has confirmed that by co-electrospinning PCL and GEL at a flow rate of 2:1 (the same preparation parameters as PCL-sim/GEL-sp membrane), an ideal mechanical barrier can be created [14]. This observation can be ascribed to the extensive interlacing and interlocking of the PCL/GEL fibers [34].

Simultaneously, GEL, a protein component within the co-electrospinning fiber network, plays a crucial role in promoting cell adhesion and enhancing the cytocompatibility of the membrane [35]. Our findings indicate a correlation between the surface structure of the membrane and initial cell adhesion. The incorporation of hierarchical micro-nanofibrous structures in the membrane improves various cellular responses, including cell viability, attachment, and proliferation. Numerous studies have demonstrated that hierarchical micro/-nanofibrous structures are well-suited for tissue regeneration and reconstruction, encompassing skin tissue, ligaments, tendons, bone tissue, and neurons [36]. Furthermore, the integration of GEL as a protein component in the membrane structure satisfies the requirements for bone tissue regeneration by providing a stable mechanical microenvironment and essential biochemical factors necessary for cell proliferation and differentiation [34]. However, despite the significant influence of membrane structures on membrane biocompatibility, their ability to induce cell homing and promote osteogenesis remains limited [37]. Consequently, a series of experiments were conducted to investigate the cell migration capacity and osteogenic differentiation activity of MSCs seeded on SP/SIM-loaded membranes.

The controlled and sustained release of SP and SIM from the membrane creates a microenvironment that mimics the natural osteogenesis events, facilitating the repair of bone defects. This controlled release

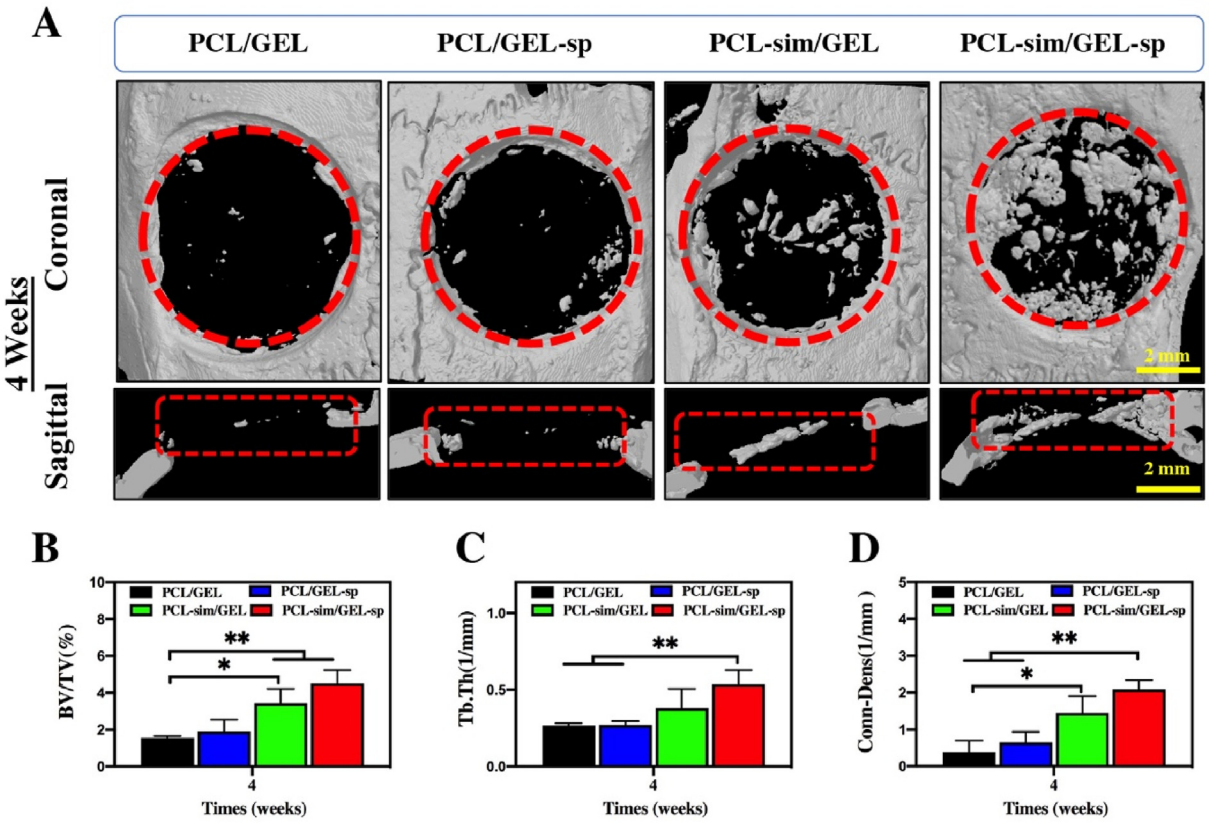

Fig. 8. Micro-CT analysis of the bone defect region one-month post-implantation. (A) Representative micro-CT reconstruction images in coronal and sagittal views. The red dotted lines marked the initial boundary of the critical cranial defect; quantitative analysis of (B) BV/TV, (C) Tb·Th, and (D) Conn-Dens in the cranial defect area after one month, $*p < 0.05$, $**p < 0.01$. (For interpretation of the references to color in this figure legend, the reader is referred to the Web version of this article.)

mechanism ensures early revascularization in the defect area and induces migration of MSCs to the wound sites. Subsequently, it provides a sustained osteogenic induction factor, ultimately leading to successful bone repair. In line with our findings, previous studies suggest that SIM has a positive effect on cell migration. Han et al. found that SIM improved cell migration and promotes neuroregeneration after spinal cord injury, potentially through upregulating BDNF and VEGF [38]. In another study, Bing et al. demonstrated that SIM enhanced cell migration through the chemokine receptor 4 signaling pathway and might have the potential to promote stem cell therapy [39]. Moreover, Song et al. found that SIM induced endothelial progenitor cells (EPCs) homing and enhanced vasculogenesis, which could promote bone defect repair [40]. Overall, these findings suggest that SIM may have beneficial effects on cell migration in different contexts and have the potential to promote tissue repair and regeneration. However, further studies are needed to fully understand the mechanism of SIM-induced cell migration and its potential therapeutic applications.

Moreover, SP is a widely used bioactive peptide that is naturally secreted from the peripheral sensory nerve fibers. Several studies have confirmed the essential role of SP in numerous biological functions, particularly its significant and direct effects on cell homing and recruitment initiation [15,41]. Osteogenic differentiation of MSCs upon reaching the site of a bone defect is a crucial step in the process of bone regeneration. However, our findings indicate that the involvement of SP did not have a significant impact on cell viability, ALP activity, and mineralization. Similar observations were made by Mu et al. who found that SP at different concentrations had a negligible effect on enhancing the osteogenic differentiation of MSCs [21]. However, upon reviewing the literature, inconsistent results were found, and clear evidence regarding the association between SP and the mechanisms involved in osteoblast differentiation is lacking [42,43]. These findings suggest that further investigations are necessary to gain a better understanding of the role of SP in osteogenic differentiation and bone reformation. In contrast, numerous *in vitro* and *in vivo* studies have extensively documented the success of SIM in promoting bone repair. For instance, Zhang et al. claimed that the SIM could upgrade the MSCs differentiation via activating the Wnt/β-catenin pathway [44]. In another study, Tai et al. reported that SIM played an essential role in maintaining the actin cytoskeleton intact and improving osteoblast cell functions, which boosted the expression of BMP-2 and RUNX-2 in MSCs. Moreover, using SIM-loaded mesoporous hydroxyapatite microspheres, Yu et al. demonstrated a superior ability to accelerate bone repair by improving osteogenesis and angiogenesis [45]. On the other hand, dozens of studies confirmed the positive involvement of SIM in promoting revascularization [18,46]. It was illustrated that SIM could enhance wound healing by upgrading the SDF1/CXCR4 pathway [47]. Moreover, there was a broad agreement that SIM has been found to have an outstanding ability to stimulate angiogenesis via activating Akt/PKB in HUVECs, thus inhibiting apoptosis and revving vascular structure formation [39]. Based on our findings, we have concluded that delivering SIM at appropriate concentrations has a direct and positive impact on angiogenesis and osteogenesis. The distinct roles and release profiles of SIM and SP in the co-electrospinning membrane contribute to their combined effect, with SP enhancing cell recruitment and SIM promoting revascularization and osteogenic differentiation. These complementary actions result in improved overall bone regeneration outcomes.

Taken together, this study presents compelling evidence regarding the mechanisms of bone regeneration, which strongly rely on the controlled release of SP and SIM facilitated by the co-electrospinning membrane. Firstly, during the early stage of bone healing, a substantial

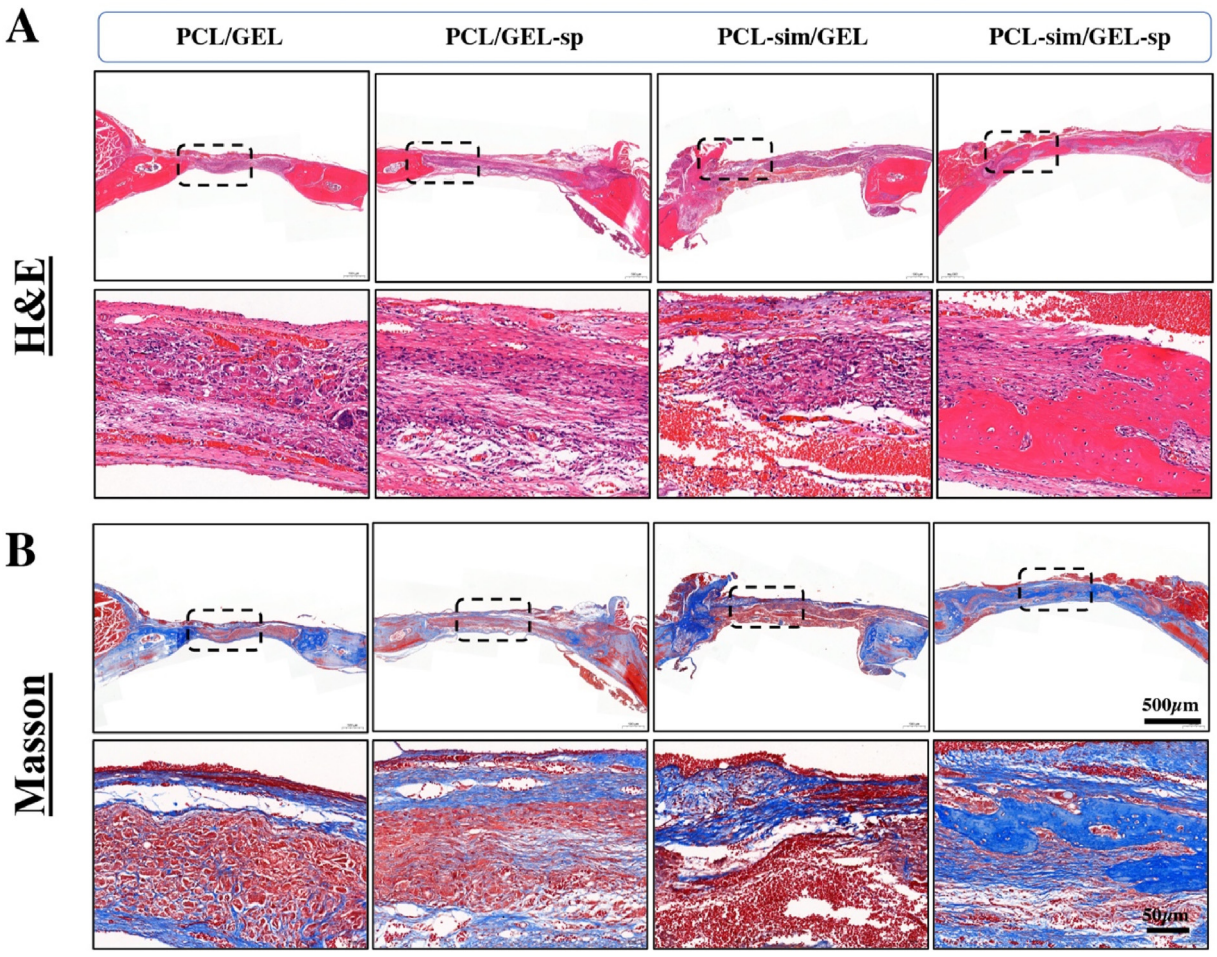

Fig. 9. Histological analysis of the bone defect region one-month post-implantation. (A) H&E and (B) Masson's trichrome staining images of the calvarial defect.

number of MSCs were recruited and stimulated to migrate to the implantation site through the release of SP from the GEL nanofiber. Subsequently, the hierarchical micro-nano structure of the targeted membrane provided a favorable environment for the initial adhesion and differentiation of MSCs. Moreover, the sustained release of SIM from the PCL fiber enhanced endothelial cell functions and promoted revascularization at the injury site, ensuring an adequate supply of nutrients. During the subsequent stage of bone remodeling, the continuous osteoinduction mediated by the sustained release of SIM from the PCL fiber significantly enhanced the osteogenic differentiation of MSCs, ultimately leading to complete bone repair.

5. Conclusion

In summary, the co-electrospinning technique successfully fabricated a hierarchical dual drug delivery system (PCL-sim/GEL-sp) with a tunable drug release function. A series of cellular experiments *in vitro* demonstrated that PCL-sim/GEL-sp membrane effectively enhanced the migration/angiogenesis of HUVECs and the recruitment/osteoblastic differentiation of MSCs. Furthermore, the *in vivo* results, including immunohistochemical staining, micro-CT scanning observation, and H&E/Masson's trichrome staining, further indicated that PCL-sim/GEL-sp membrane could significantly stimulate cell recruitment, revascularization, and osteogenesis, thus accelerating the bone regeneration process. In conclusion, our results advance our knowledge of co-electrospinning membranes and lay the groundwork for potential clinical applications.

Author contributions

Xinkun Shen, Pingping Ma, and Jinsong Liu contributed to the conceptualization and design of this study, performed formal analysis, acquired funding, provided resources, supervised the project, and contributed to writing the final draft, as well as reviewing and editing it. Mohammed A. Al-Baadani and Lihua Xu conducted the investigation and experiments, including the fabrication of the scaffolds, physico-chemical characterization, and *in vitro* and *in vivo* biological experiments and contributed to the original draft of the manuscript. Kexin Cai and Kendrick Hii Ru Yie participated in the statistical analysis and release studies. Yiding Shen and Abdullrahman Al-Bishari assisted with confocal and scanning electron microscopy experiments. Bilal A. Al-Shaaobi contributed to the resources related to *in vivo* assessment. All authors revised and edited the draft, and read and approved the final manuscript."

Declaration of competing interest

The authors declare that they have no known competing financial interests or personal relationships that could have appeared to influence the work reported in this paper.

Data availability

Data will be made available on request.

Acknowledgments

M.A. Al-Baadani, L. Xu contributed equally to this work. This work was funded by National Natural Science Foundation of China (82071170, 81870810 and 82171004), Zhejiang Provincial Science and Technology Project for Public Welfare (LY21H180006 and LGF21H140004), Key Technological Innovation Projects of Wenzhou (ZY2019009), Wenzhou Public Welfare Science and Technology Project (Y20190099), Wenzhou Medical University Basic Scientific Research Operating Expenses (KYYW201905).

Appendix A. Supplementary data

Supplementary data to this article can be found online at https://doi.org/10.1016/j.mtbio.2023.100692.

References

[1] M. Retzepi, N. Donos, Guided bone regeneration: biological principle and therapeutic applications, Clin. Oral Implants Res. 21 (6) (2010) 567–576.
[2] P. Gentile, V. Chiono, C. Tonda-Turo, A.M. Ferreira, G. Ciardelli, Polymeric membranes for guided bone regeneration, Biotechnol. J. 6 (10) (2011) 1187–1197.
[3] M. Kikuchi, Y. Koyama, T. Yamada, Y. Imamura, T. Okada, N. Shirahama, K. Akita, K. Takakuda, J. Tanaka, Development of guided bone regeneration membrane composed of β-tricalcium phosphate and poly (L-lactide-co-glycolide-co-ε-caprolactone) composites, Biomaterials 25 (28) (2004) 5979–5986.
[4] J. Wang, L. Wang, Z. Zhou, H. Lai, P. Xu, L. Liao, J. Wei, Biodegradable polymer membranes applied in guided bone/tissue regeneration: a review, Polymers 8 (4) (2016) 115.
[5] A. Sculean, D. Nikolidakis, F. Schwarz, Regeneration of periodontal tissues: combinations of barrier membranes and grafting materials–biological foundation and preclinical evidence: a systematic review, J. Clin. Periodontol. 35 (2008) 106–116.
[6] M.A. Al-Baadani, L. Xu, K.H.R. Yie, A. Sun, X. Gao, K. Cai, B.A. Al-Shaaobi, A.M. Al-Bishari, L. Cai, X. Shen, In situ preparation of alendronate-loaded ZIF-8 nanoparticles on electrospun nanofibers for accelerating early osteogenesis in osteoporosis, Mater. Design (2022), 110596.
[7] M. He, Q. Wang, L. Xie, H. Wu, W. Zhao, W. Tian, Hierarchically multi-functionalized graded membrane with enhanced bone regeneration and self-defensive antibacterial characteristics for guided bone regeneration, Chem. Eng. J. 398 (2020), 125542.
[8] P. Gentile, A.M. Ferreira, J.T. Callaghan, C.A. Miller, J. Atkinson, C. Freeman, P.V. Hatton, Multilayer nanoscale encapsulation of biofunctional peptides to enhance bone tissue regeneration in vivo, Adv. Healthc. Mater. 6 (8) (2017), 1601182.
[9] Y. Wang, Y. Jiang, Y. Zhang, S. Wen, Y. Wang, H. Zhang, Dual functional electrospun core-shell nanofibers for anti-infective guided bone regeneration membranes, Mater. Sci. Eng. C 98 (2019) 134–139.
[10] B. McKibbin, The biology of fracture healing in long bones, the Journal of bone and joint surgery, British 60 (2) (1978) 150–162.
[11] L. Cheng, Z. Chen, Z. Cai, J. Zhao, M. Lu, J. Liang, F. Wang, J. Qi, W. Cui, L. Deng, Bioinspired functional black phosphorus electrospun fibers achieving recruitment and biomineralization for staged bone regeneration, Small 16 (50) (2020), 2005433.
[12] Y. Mao, Y. Chen, W. Li, Y. Wang, J. Qiu, Y. Fu, J. Guan, P. Zhou, Physiology-inspired multilayer nanofibrous membranes modulating endogenous stem cell recruitment and osteo-differentiation for staged bone regeneration, Adv. Healthc. Mater. 11 (21) (2022), 2201457.
[13] Y.S. Liu, M.E. Ou, H. Liu, M. Gu, L.W. Lv, C. Fan, T. Chen, X.H. Zhao, C.Y. Jin, X. Zhang, Y. Ding, Y.S. Zhou, The effect of simvastatin on chemotactic capability of SDF-1α and the promotion of bone regeneration, Biomaterials 35 (15) (2014) 4489–4498.
[14] M.A. Al-Baadani, K.H.R. Yie, A.M. Al-Bishari, B.A. Alshobi, Z. Zhou, K. Fang, B. Dai, Y. Shen, J. Ma, J. Liu, Co-electrospinning polycaprolactone/gelatin membrane as a tunable drug delivery system for bone tissue regeneration, Mater. Design (2021), 109962.
[15] M.J. Kim, Y.B. Ji, J.Y. Seo, S.H. Park, J.H. Kim, B.H. Min, M.S. Kim, Substance P-loaded electrospun small intestinal submucosa/poly (ε-caprolactone)-ran-poly (L-lactide) sheet to facilitate wound healing through MSC recruitment, J. Mater. Chem. B 7 (47) (2019) 7599–7611.
[16] H.S. Hong, J. Lee, E. Lee, Y.S. Kwon, E. Lee, W. Ahn, M.H. Jiang, J.C. Kim, Y. Son, A new role of substance P as an injury-inducible messenger for mobilization of CD29+ stromal-like cells, Nat. Med. 15 (4) (2009) 425–435.
[17] J.T. Christenson, Preoperative lipid-control with simvastatin reduces the risk of postoperative thrombocytosis and thrombotic complications following CABG, Eur. J. Cardio. Thorac. Surg. 15 (4) (1999) 394–400.
[18] J.R. Alhamdi, T. Peng, I.M. Al-Naggar, K.L. Hawley, K.L. Spiller, L.T. Kuhn, Controlled M1-to-M2 transition of aged macrophages by calcium phosphate coatings, Biomaterials 196 (2019) 90–99.
[19] A. Bitto, L. Minutoli, D. Altavilla, F. Polito, T. Fiumara, H. Marini, M. Galeano, M. Calò, P. Lo Cascio, M. Bonaiuto, A. Migliorato, A.P. Caputi, F. Squadrito, Simvastatin enhances VEGF production and ameliorates impaired wound healing in experimental diabetes, Pharmacol. Res. 57 (2) (2008) 159–169.
[20] H. Pullisaar, J.E. Reseland, H.J. Haugen, J.E. Brinchmann, E. Østrup, Simvastatin coating of TiO2 scaffold induces osteogenic differentiation of human adipose tissue-derived mesenchymal stem cells, Biochem. Biophys. Res. Commun. 447 (1) (2014) 139–144.
[21] C. Mu, Y. Hu, Y. Hou, M. Li, Y. He, X. Shen, B. Tao, C. Lin, M. Chen, M. Chen, Substance P-embedded multilayer on titanium substrates promotes local osseointegration via MSC recruitment, J. Mater. Chem. B 8 (6) (2020) 1212–1222.
[22] L. Huang, Z. Luo, Y. Hu, X. Shen, M. Li, L. Li, Y. Zhang, W. Yang, P. Liu, K. Cai, Enhancement of local bone remodeling in osteoporotic rabbits by biomimic multilayered structures on T i6 A l4 V implants, J. Biomed. Mater. Res. 104 (6) (2016) 1437–1451.
[23] S. Wu, X. Shen, M. Chen, K.H.R. Yie, Z. Zhou, M.A. Al-Baadani, K. Fang, A.M. Al-Bishari, Z. Deng, J. Liu, Multifunctional TaCu-nanotubes coated titanium for enhanced bacteriostatic, angiogenic and osteogenic properties, Mater. Sci. Eng. C 120 (2021), 111777.
[24] Y. Liu, Z. Zhu, X. Pei, X. Zhang, X. Cheng, S. Hu, X. Gao, J. Wang, J. Chen, Q. Wan, ZIF-8-Modified multifunctional bone-adhesive hydrogels promoting angiogenesis and osteogenesis for bone regeneration, ACS Appl. Mater. Interfaces 12 (33) (2020) 36978–36995.
[25] H.W. Lam, H.C. Lin, S.C. Lao, J.L. Gao, S.J. Hong, C.W. Leong, P.Y.K. Yue, Y.W. Kwan, A.Y.H. Leung, Y.T. Wang, The angiogenic effects of Angelica sinensis extract on HUVEC in vitro and zebrafish in vivo, J. Cell. Biochem. 103 (1) (2008) 195–211.
[26] G. Carpentier, S. Berndt, S. Ferratge, W. Rasband, M. Cuendet, G. Uzan, P. Albanese, Angiogenesis Analyzer for imageJ—a comparative morphometric analysis of "endothelial tube formation Assay" and "fibrin Bead Assay", Sci. Rep. 10 (1) (2020) 1–13.
[27] M.H. El-Newehy, S.S. Al-Deyab, E.-R. Kenawy, A. Abdel-Megeed, Fabrication of electrospun antimicrobial nanofibers containing metronidazole using nanospider technology, Fibers Polym. 13 (6) (2012) 709–717.
[28] J. Wu, Z. Zhang, W. Zhou, X. Liang, G. Zhou, C.C. Han, S. Xu, Y. Liu, Mechanism of a long-term controlled drug release system based on simple blended electrospun fibers, J. Contr. Release 320 (2020) 337–346.
[29] Q. Liu, W.-C. Ouyang, X.-H. Zhou, T. Jin, Z.-W. Wu, Antibacterial activity and drug loading of moxifloxacin-loaded poly (vinyl alcohol)/chitosan electrospun nanofibers, Front. Mater. Sci. China 8 (2021), 643428.
[30] Y.J. Son, W.J. Kim, H.S. Yoo, Therapeutic applications of electrospun nanofibers for drug delivery systems, Arch Pharm. Res. (Seoul) 37 (2014) 69–78.
[31] H.M. Hashem, A. Motawea, A.H. Kamel, E.A. Bary, S.S. Hassan, Fabrication and characterization of electrospun nanofibers using biocompatible polymers for the sustained release of venlafaxine, Sci. Rep. 12 (1) (2022), 18037.
[32] J.A. Cottrell, J.C. Turner, T.L. Arinzeh, J.P. O'Connor, The biology of bone and ligament healing, Foot Ankle Clin. 21 (4) (2016) 739–761.
[33] A. Nasajpour, S. Ansari, C. Rinoldi, A.S. Rad, T. Aghaloo, S.R. Shin, Y.K. Mishra, R. Adelung, W. Swieszkowski, N. Annabi, A multifunctional polymeric periodontal membrane with osteogenic and antibacterial characteristics, Adv. Funct. Mater. 28 (3) (2018), 1703437.
[34] L. Wu, Y. Gu, L. Liu, J. Tang, J. Mao, K. Xi, Z. Jiang, Y. Zhou, Y. Xu, L. Deng, Hierarchical micro/nanofibrous membranes of sustained releasing VEGF for periosteal regeneration, Biomaterials 227 (2020), 119555.
[35] K. Qin, F. Wang, R.M. Simpson, X. Zheng, H. Wang, Y. Hu, Z. Gao, Q. Xu, Q. Zhao, Hyaluronan promotes the regeneration of vascular smooth muscle with potent contractile function in rapidly biodegradable vascular grafts, Biomaterials 257 (2020), 120226.
[36] X. Feng, J. Li, X. Zhang, T. Liu, J. Ding, X. Chen, Electrospun polymer micro/nanofibers as pharmaceutical repositories for healthcare, J. Contr. Release 302 (2019) 19–41.
[37] S. Ren, Y. Zhou, K. Zheng, X. Xu, J. Yang, X. Wang, L. Miao, H. Wei, Y. Xu, Cerium oxide nanoparticles loaded nanofibrous membranes promote bone regeneration for periodontal tissue engineering, Bioact. Mater. 7 (2022) 242–253.
[38] X. Han, N. Yang, Y. Cui, Y. Xu, G. Dang, C. Song, Simvastatin mobilizes bone marrow stromal cells migrating to injured areas and promotes functional recovery after spinal cord injury in the rat, Neurosci. Lett. 521 (2) (2012) 136–141.
[39] W. Bing, X. Pang, Q. Qu, X. Bai, W. Yang, Y. Bi, X. Bi, Simvastatin improves the homing of BMSC s via the PI 3K/AKT/miR-9 pathway, J. Cell Mol. Med. 20 (5) (2016) 949–961.
[40] Q. Song, L. Wang, J. Zhu, X. Han, X. Li, Y. Yang, Y. Sun, C. Song, Effect of simvastatin on inducing endothelial progenitor cells homing and promoting bone defect repair, Zhongguo xiu fu Chong Jian wai ke za zhi= Zhongguo Xiufu Chongjian Waike Zazhi= Chinese J. Reparat. Reconstruct. Surg. 24 (9) (2010) 1103–1106.
[41] A. Mashaghi, A. Marmalidou, M. Tehrani, P.M. Grace, C. Pothoulakis, R. Dana, Neuropeptide substance P and the immune response, Cell. Mol. Life Sci. 73 (22) (2016) 4249–4264.
[42] F.X.Z. Li, F. Xu, X. Lin, F. Wu, J.Y. Zhong, Y. Wang, B. Guo, M.H. Zheng, S.K. Shan, L.Q. Yuan, The role of substance P in the regulation of bone and cartilage metabolic activity, Front. Endocrinol. 11 (2020) 77.
[43] L. Wang, S. Hou, I. Sabsovich, T.-Z. Guo, T. Wei, W.S. Kingery, Mice lacking substance P have normal bone modeling but diminished bone formation, increased resorption, and accelerated osteopenia with aging, Bone 144 (2021), 115806.
[44] M. Zhang, Y.Q. Bian, H.M. Tao, X.F. Yang, W.D. Mu, Simvastatin induces osteogenic differentiation of MSCs via Wnt/β-catenin pathway to promote fracture healing, Eur. Rev. Med. Pharmacol. Sci. 22 (9) (2018) 2896–2905.

[45] H. Jin, Y. Ji, Y. Cui, L. Xu, H. Liu, J. Wang, Simvastatin-incorporated drug delivery systems for bone regeneration, ACS Biomater. Sci. Eng. 7 (6) (2021) 2177–2191.
[46] J. Mohajer Ansari, P. Ramhormozi, R. Shabani, H. Pazoki-Toroudi, A. Yari, M. Barati, M. Dahmardehei, A. Babakhani, M. Nobakht, Simvastatin combined with bone marrow mesenchymal stromal cells (BMSCs) improve burn wound healing by ameliorating angiogenesis through SDF-1α/CXCR4 pathway, Iran. J. Basic Med. Sci. 23 (6) (2020) 751–759.
[47] H. Wu, H. Jiang, D. Lu, C. Qu, Y. Xiong, D. Zhou, M. Chopp, A. Mahmood, Induction of angiogenesis and modulation of vascular endothelial growth factor receptor-2 by simvastatin after traumatic brain injury, Neurosurgery 68 (5) (2011) 1363–1371, discussion 1371.